Published in final edited form as:
Nat Chem Biol. 2024 June ; 20(6): 673–688. doi:10.1038/s41589-024-01593-6.

Structures, mechanisms and applications of RNA-centric CRISPR–Cas13

Hui Yang[1,✉], **Dinshaw J. Patel**[2,✉]

[1]Key Laboratory of RNA Innovation, Science and Engineering, Shanghai Institute of Biochemistry and Cell Biology, Center for Excellence in Molecular Cell Science, Chinese Academy of Sciences, University of Chinese Academy of Sciences, Shanghai, China.

[2]Structural Biology Program, Memorial Sloan Kettering Cancer Center, New York, NY, USA.

Abstract

Prokaryotes are equipped with a variety of resistance strategies to survive frequent viral attacks or invading mobile genetic elements. Among these, CRISPR–Cas surveillance systems are abundant and have been studied extensively. This Review focuses on CRISPR–Cas type VI Cas13 systems that use single-subunit RNA-guided Cas endonucleases for targeting and subsequent degradation of foreign RNA, thereby providing adaptive immunity. Notably, distinct from single-subunit DNA-cleaving Cas9 and Cas12 systems, Cas13 exhibits target RNA-activated substrate RNase activity. This Review outlines structural, biochemical and cell biological studies toward elucidation of the unique structural and mechanistic principles underlying surveillance effector complex formation, precursor CRISPR RNA (pre-crRNA) processing, self-discrimination and RNA degradation in Cas13 systems as well as insights into suppression by bacteriophage-encoded anti-CRISPR proteins and regulation by endogenous accessory proteins. Owing to its programmable ability for RNA recognition and cleavage, Cas13 provides powerful RNA targeting, editing, detection and imaging platforms with emerging biotechnological and therapeutic applications.

In many bacteria and most archaea, CRISPR–Cas systems provide adaptive immunity by acquiring immune memory against previous invading mobile genetic elements and harnessing RNA-guided programmable endonucleases for foreign nucleic acid degradation. A typical CRISPR–Cas system consists of a genetic locus of related *cas* genes and a CRISPR array containing several different spacer units flanked by unique direct repeats (Figs. 1 and 2). The arms race between bacteria and phages triggers activation of

✉ **Correspondence and requests for materials** should be addressed to Hui Yang or Dinshaw J. Patel. yanghui@sibcb.ac.cn; pateld@mskcc.org.

Author contributions
H.Y. wrote the initial draft and prepared the figures of the review.
D.J.P. provided input and assistance in completing the review.

Competing interests
The authors declare no competing interests.

Supplementary information The online version contains supplementary material available at https://doi.org/10.1038/s41589-024-01593-6.

Peer review information *Nature Chemical Biology* thanks Songying Ouyang and the other, anonymous, reviewer(s) for their contribution to the peer review of this work.

highly diverse CRISPR loci and Cas proteins, leading to divergent immune mechanisms. Conversely, phages have evolved divergent bacteriophage- or prophage-encoded anti-CRISPR proteins (Acrs) that inhibit Cas effector complex-mediated targeting of invading nucleic acids (reviewed in refs. 1–11).

Despite the diversity and complexity of CRISPR–Cas systems, the immunization process functions in three stages: adaptation, expression and interference (reviewed in refs. 12–18) (Fig. 1). At the initial adaptation stage, short DNA fragments derived from phages or invading plasmids, called protospacers, are integrated into the leader proximal end of a host CRISPR array to create new spacer segments, which provide immunological memory of previous infections (reviewed in refs. 18–22). In many cases, spacer acquisition is mediated by the Cas1–Cas2 integrase complex and sometimes is also associated with reverse transcriptase (RT), Cas4 or Csn2. At the subsequent expression stage, the CRISPR array is transcribed into a single noncoding RNA, known as pre-crRNA, and further processed by related Cas proteins or non-Cas host RNases to generate individual mature CRISPR RNA (crRNA), each of which carries a single spacer together with one adjacent direct repeat[23–25]. At the last interference stage, a surveillance ribonucleoprotein complex, called the effector or interference complex, formed by mature crRNA and effector Cas protein(s), recognizes and cleaves foreign nucleic acids that contain sequences complementary to the spacer segments of crRNA[26–28].

Based on the protein constituents of effector modules, locus architectures and *cas* gene composition, CRISPR–Cas systems are grouped into two classes and further subclassified into six types, labeled I to VI[29]. Class 1 systems (types I, III and IV) use multiple (typically three to six) Cas subunits to form a multisubunit effector complex for interference[30]. By contrast, class 2 systems (types II, V and VI) use a single, relatively larger, multiple-domain-containing Cas protein for degradation of invading nucleic acids[31,32].

RNA-centric type VI Cas13

Unlike DNA-targeting systems that could repress virus replication by a single cleavage of viral DNA, RNA-targeting systems need to repel multiple copies of RNA transcripts to achieve immunity. RNA-targeting type VI CRISPR–Cas Cas13 effectors monitor RNA in the host cell and search for RNA targets that are complementary with the crRNA spacer (Fig. 1). Beyond degradation of bound RNA targets, Cas13 is also activated by bound RNA targets, thereby inducing collateral degradation of nonspecific substrate single-stranded RNA (ssRNA) (Fig. 1). Such processes provide immunity against complementary viral or phage RNA targets and cognate DNA phage transcripts, thereby inducing cell dormancy of infected cells, together with neutralization of CRISPR-resistant phages[33–36] (reviewed in ref. 37). Various accessory proteins are found in CRISPR–Cas13 loci (Fig. 2) and are believed to regulate Cas13 activity[33,38].

The capacity of a single Cas protein for recognition and cleavage of target ssRNA, in addition to target-dependent collateral RNase activity of Cas13, in turn empowers applications for programmable RNA targeting, editing, tracking, detection and imaging in both prokaryotic and eukaryotic cells[39–43].

We will describe the current understanding of the three stages of the immunization process mediated by type VI Cas13 systems, with an emphasis on the expression and interference steps, thereby providing up-to-date knowledge of structure-based mechanistic insights into the function and behavior of single-subunit Cas13 proteins during effector complex formation, crRNA maturation, self versus non-self discrimination, substrate recognition and cleavage and activity modulation. Throughout, we will also outline recent advances together with remaining challenges toward the development of powerful and programmable Cas13-based RNA manipulation applications.

Classification and composition

Searches for putative CRISPR–Cas type VI loci led to the discovery of subtypes VI-A, VI-B (including VI-B1 and VI-B2), VI-C and VI-D as well as VI-BT and VI-CT from distinct branches within subtypes VI-B and VI-C[32–34,38,44–46] (Fig. 2 and Supplementary Table 1). The classification of subtypes is based on subtler differences in locus organization, Cas13 phylogeny and the positions of the pair of conserved HEPN domains in Cas13. Different Cas13 orthologs exhibit extremely low sequence similarity but share a similar overall bilobed architecture common to other members of the single-subunit Cas protein family, consisting of recognition (REC) and nuclease (NUC) lobes. Generally, the REC lobe is composed of N-terminal (NTD) and helical-1 domains that mainly contribute to crRNA recognition, while the NUC lobe is composed of helical-2, split HEPN-1 and HEPN-2 domains that mainly contribute to target RNA accommodation and cleavage. Extra domains include the helical-3 (or linker) domain in type VI-A and RRI (or lid) domain in type VI-B (Supplementary Table 2).

Spacer acquisition is undefined among type VI systems, with little known about how Cas13 systems acquire new spacers and whether the acquisition is from RNA or DNA. Crosstalk on adaptation was observed between co-occurring RNA-targeting type VI-B and DNA-targeting type II-C CRISPR–Cas systems[47], suggesting that RNA-targeting systems provide protection to overcome DNA-based immunity evasion. Details and underlying mechanisms on co-occurring RNA-targeting and DNA-targeting systems remain to be explored.

crRNA biogenesis in type VI systems

In type VI systems, pre-crRNA processing activity is relegated to effector modules within Cas13 proteins, with a requirement for formation of the CRISPR immune surveillance complex (Fig. 1).

CRISPR array organization and crRNA topology

The CRISPR arrays in different subtypes show unique and conserved features related to length and sequence (Supplementary Table 1), resulting in a defined predicted secondary structure (zoomed-in box in Fig. 1). Generally, the direct repeat contains a stem loop (also called the 5′-handle), flanked by the processing cleavage site at one side and a variant spacer at the other side (reviewed in refs. 48,49). The upstream and downstream regions of the stem loop, called 5′- and 3′-flank segments, exhibit single-stranded conformations with distinct lengths in different subtypes. The pre-crRNA processing sites within the

direct repeat as well as the dependence on divalent metal ions are different among subtypes[33,34,38,50,51] and sometimes distinct even across different species within the same subtype[50,52,53] (Supplementary Table 1), which highlights a notable mechanistic distinction between different subtypes.

crRNA recognition and maturation

The recognition of crRNA in types VI-A, VI-B and VI-D has been studied in great detail[51–60] (reviewed in ref. 49), with the focus below on the type VI-A system. Structural studies have been undertaken on U-cleaving *Leptotrichia shahii Lsh*Cas13 (Fig. 3a) in the apo state (Fig. 3b) and bound to crRNA (Fig. 3c–e).

Cas13 buries the stem-loop of the direct repeat in the cleft between the NTD and helical-1 domains of the REC lobe (Fig. 3c–e). The stem region of crRNA is recognized mainly by backbone contacts with Cas13 residues, whereas the loop segment adopts a distinct conformation with extrusion out of two to four nucleotides, some of which are recognized in a sequence-specific manner. The 3′-flank segment exhibits a nearly A-form conformation and is stabilized by ribose–phosphate backbone interactions with the HEPN-2 domain. Substitution of nucleotides in the bulge, loop or flanking regions of the stem as well as structural mutations within the stem-loop region abolishes pre-crRNA processing and target RNA cleavage, due to failure of RNP complex formation between Cas13 and crRNA[36,50,53].

The spacer region is bound in a non-sequence-specific manner. Before base pairing of target RNA with the crRNA spacer, several regions of spacer are invisible in the binary structure due to high flexibility (Fig. 3c–e). The central and 3′-segments of the spacer (the repeat region-distal segment) are solvent accessible and adopt a nearly A-form conformation, which allows for target searching and loading[49,51,54,55,58–60].

Upon binding crRNA, domain rearrangements occur in the two lobes to generate an RNA-binding cleft[51,54] (Fig. 3e). The Cas13a helical-2 domain moves toward the linker domain in the NUC lobe on complex formation (Fig. 3e), resulting in a more compact conformation and a channel for crRNA accommodation[54] (Fig. 3e,f).

On the behavior of pre-crRNA cleavage, Cas13a generates a 2′,3′-cyclic phosphate on the 5′-flank product and a 5′-OH on the mature crRNA, with the mature crRNA bound to Cas13 after processing[38,50]. The 5′-flank segment usually presents a non-A-form conformation and is positioned in the groove between the helical-1 and HEPN-2 domains, with some nucleotides in this region contributing to the sequence specificity of bound crRNA[54]. In crRNA-bound *Lsh*Cas13, the conserved Arg438 and the nonconserved Lys441 and Lys471 residues in the helical-1 domain has key roles in cleavage chemistry (Fig. 3f), given that Ala substitutions at these positions severely impacted pre-crRNA processing. By contrast, Ala substitution of residues surrounding the scissile nucleotide (−27 position) in the HEPN-2 domain (Fig. 3f) showed little effect on pre-crRNA cleavage[54]. Interestingly, structural and biochemical data on U-cleaving *Leptotrichia buccalis Lbu*Cas13a and A-cleaving *Lachnospiraceae bacterium Lba*Cas13a suggest a conserved processing mechanism involving the helical-1 and HEPN-2 domains, with the surrounding conserved residues

forming an acid–base catalytic center[50,52–55], which shows divergence from U-cleaving *Lsh*Cas13a.

Notably, Cas13 executes pre-crRNA cleavage and target RNA cleavage by using two distinct catalytic pockets (Fig. 3a,f). The two conserved R-$X_{4–6}$-H motifs in the two HEPN domains are responsible for target RNA cleavage but have no effect on pre-crRNA cleavage.

Interference mediated by Cas13

When mature crRNA is loaded into Cas13, this ribonucleoprotein complex retains the inactive state and is ready to monitor the presence of foreign invaders to provide RNA immunity. Cas13 is activated only upon binding with target ssRNA containing a region complementary with the crRNA spacer. The target RNA is then cleaved at promiscuous positions outside the guide–target duplex[34,36,60]. Before the release of the crRNA-bound segment, Cas13 collaterally cleaves environmental nonspecific ssRNA, resulting in cell dormancy or cell death. Sequence-specific target RNA cleavage (called *cis*-RNase activity) and collaterally nonspecific RNA cleavage (called collateral *trans*-RNase activity) are executed by the pair of R-$X_{4–6}$-H motifs in the HEPN domains, which is a general property of type VI systems. Cas13 lacks the capacity to open up double-stranded RNA, and thus the cleavage pattern is determined by nucleotide cleavage preference (details in Supplementary Table 1) and structurally accessible ssRNA regions[34,36,51–53,55].

Sequence-specific target RNA cleavage

Structural studies have been undertaken on U-cleaving *Lbu*Cas13a (Fig. 4a) bound to crRNA[55] (Fig. 4b,d) and on the addition of complementary target RNA[55] (Fig. 4c,e). The REC lobe binds to the crRNA direct repeat, while the NUC lobe forms an RNA duplex-binding channel to accommodate the guide–target RNA duplex (Fig. 4c). Notably, on target RNA binding, conformational changes occur in the 3′-flank of the crRNA direct repeat (Fig. 4d–g). Before target RNA loading, the three nucleotides (−1 to −3) in the 3′-flank that are connected with the spacer adopt a pre-ordered A-form conformation[55] (Fig. 4d). Upon target RNA access, these three nucleotides (−1 to −3) in the 3′-flank move toward the crRNA stem loop and form a kink (Fig. 4e,f). Simultaneously, target RNA induces substantial conformational changes in the helical-2 and HEPN-1 protein components of Cas13a (Fig. 4f,g), thereby generating both the positively charged binding channel to accommodate the guide–target RNA duplex (Fig. 4f) and the activated composite HEPN catalytic pocket for both *cis*- and collateral *trans* RNA cleavage (Fig. 4g)[51,54,55]. The channel for guide–target RNA duplex accommodation is widened, and the residues in the positively charged surface make backbone interactions mainly with the central region of the duplex, with a few backbone interactions also formed in the repeat-proximal and repeat-distal regions (Fig. 4f). Focusing on the composite HEPN catalytic pocket responsible for RNase activity, the distance among the four key catalytic residues (two arginines and two histidines) in the strictly conserved R-$X_{4–6}$-H motifs in the two HEPN domains is shortened on complex formation with target RNA due to the movement of the HEPN-1 domain toward the surface and proximal to the HEPN-2 domain (Fig. 4g), making Cas13 catalytically active for ssRNA hydrolysis. Although there is no structure of ssRNA positioned in the

composite HEPN pocket yet, it has been proposed, in terms of a catalytic mechanism, that the conserved His acts as a general base to activate the 2′-OH, which then targets the phosphodiester backbone, with the conserved Arg in turn stabilizing the pentavalent transition state intermediate.

Mismatches in the guide–target duplex segment affect both in vitro and in vivo RNase activities. Usually, Cas13, which could somewhat tolerate a single-nucleotide mismatch, is dramatically affected by two tandem mismatches[36,44,52,54,55,58,61–63]. The most sensitive mismatch region is usually located within the central region of the spacer[36,61–63] (Supplementary Table 1), which is defined as the seed region. The seed region is consistent with the observed solvent-accessible region of the spacer in Cas13–crRNA binary complexes and extends further in some cases[49,51,54,55,58–60].

Collateral nonspecific RNA cleavage

The crRNA-bound portion of target RNA is not cleaved when it base pairs with crRNA[34,36,60], which indicates that Cas13 remain active before the guide–target duplex is unwound and the next new target RNA gains access (Fig. 1). This enables broad immunity against viral transcripts that are not recognized by crRNA or escape from DNA immunity.

In all available Cas13 structures, the catalytic pocket is solvent accessible and positioned away from the guide–target RNA duplex (Fig. 4c), thereby allowing access of the region in target RNA beyond the paired complementary portion and surrounding RNA in a non-sequence-specific manner, which explains the promiscuous cleavage site and target-dependent *cis*- and nonspecific *trans*-cleavage activity. So far, no structure is available of Cas13 bound simultaneously to crRNA, target RNA and nonspecific RNA, thereby limiting our knowledge of RNA substrate positioning. Therefore, whether sequence-specific and nonspecific target RNA species access the catalytic pocket using the same path remains unclear. Surface mutations in *Ruminococcus flavefaciens* XPD3002 Cas13d (*Rfx*Cas13d, also called CasRx) generated a variant with high sequence-specific cleavage and reduced collateral cleavage in HEK293 cells[64]. Notably, this variant exhibited reduced in vitro target-dependent *cis*- and nonspecific *trans*-cleavage activities, suggesting a global defect in the HEPN domains. It remains unclear whether there is a way to modulate sequence-specific and nonspecific RNase activities separately.

Very few studies have been done to investigate the preference of non-sequence-specific RNA targeting and the effects of global RNA degradation. It has been proposed that *Lsh*Cas13-mediated collateral cleavage of tRNA occurs at anticodon loops, thereby resulting in suppression of translation and cell dormancy[65]. In addition, massive cleavage of tRNA leads to ribosome stalling, which in turn activates type II toxin RNases that cleave mRNA and 16S ribosomal RNA, further abrogating protein synthesis[65].

Self–non-self-discrimination

The ability to discriminate invading foreign elements (non-self) from intrinsic components (self), thereby preventing self-targeting, is usually imperative for successful immune systems. Whether self–non-self-discrimination naturally occurs in Cas13 systems in their native hosts remains unclear. Some Cas13a[36], Cas13b[33] and Cas13bt[45] systems show

preference for a short sequence adjacent to the guide–target duplex, termed the protospacer flanking sequence (PFS), which drives PFS-dependent RNA targeting in vitro and in *Escherichia coli* cells but not in mammalian cells (Supplementary Table 1). The accurate mechanism underlying PFS preference and the related biological function in native host cells remain unclear.

In type VI-A *Lbu*Cas13a, *Listeria seeligeri Lse*Cas13a and *Lsh*Cas13a systems, 5–8-bp pairing between the 5′ of the direct repeat flanking spacer (called the 5′ tag) and the 3′ extended region of the target RNA flanking region complementary to the spacer segment (called the anti-tag) abolished both *cis* and *trans* RNA cleavage activities and impaired Cas13a-mediated knockdown in bacterial cells, indicating that tag–anti-tag complementarity inhibits self-targeting in native bacteria[66,67]. The structure of the U-cleaving *Lsh*Cas13a (Fig. 5a) bound to anti-tag target RNA (Fig. 5b) highlights the bound crRNA–anti-tag RNA alignment[67] (Fig. 5c). Structural data reveal that tag–anti-tag base pairing induces conformational changes of the crRNA tag region and domain movements in the NUC lobe (Fig. 5c), thereby blocking the formation of a composite HEPN catalytic pocket required for RNA cleavage activity[67] (Fig. 5d). Thus, the composite HEPN pocket adopts a noncatalytic conformation following tag–anti-tag pairing in the ternary complex (Fig. 5d), thereby preventing cleavage of self-RNA, but adopts a catalytically competent conformation when this segment is unpaired, resulting in cleavage of non-self-RNA (Fig. 4g), providing a structural explanation for self–non-self-discrimination. We anticipate that the pre-ordered 3′-flank may adopt a favorable alignment for detection and nucleation with anti-tag during self–non-self-discrimination and stronger inhibition would result from formation of tag–anti-tag base pairing.

Regulation of Cas13 RNase activity

It has been shown that Cas13-mediated immunity can be modulated by other factors including endogenous accessory proteins and phage-encoded Acrs. These proteins repress or enhance Cas13 RNase activities either through physical interactions or crosstalk with other potential signaling pathways.

Regulation by endogenous accessory proteins

Given the profound consequences of global RNA degradation, it becomes necessary to tightly control Cas13 activity. One approach relies on sufficient base pairing between target RNA and the crRNA spacer region, low mismatches in the central seed region and preferential tag–anti-tag base pairing in Cas13a systems. The alternative approach relies on intrinsic accessory proteins in CRISPR–Cas loci. Accessory genes encoding Csx27, Csx28 and WYL (named for three conserved amino acids found in a subset of domains of this superfamily) domain-containing proteins (WYL1 and WYL-b (WYL-b1–WYL-b5)) were found in types VI-B1, VI-B2 and VI-D loci, respectively[33,38] (Figs. 2 and 6a). These accessory proteins share no similarity in primary sequence and domain organization, indicating divergent modulation mechanisms of type VI effectors.

Csx27, which contains two to four predicted transmembrane helices (an AlphaFold2 model of *Bz*Csx27 is shown in Fig. 6b), was shown to repress *Prevotella buccae Pb*Cas13b-

and *Bergeyella zoohelcum Bz*Cas13b-mediated interference activity in vivo, implying that Csx27 may perform general regulatory effects and function across multiple VI-B1 loci[33,68]. However, *Bz*Csx27 was not membrane associated when expressed in *E. coli*, indicating that additional unknown factor(s) in the native hosts of VI-B1 systems might be essential for membrane localization. The accurate role and repression mechanism of Csx27 remain to be determined. Bioinformatic analysis of the neighboring genes located both upstream and downstream of the Csx27-encoding gene suggest that Csx27 might form a membrane channel and associate with natural competence or ubiquitin signaling, where it may bind with Cas13b and keep Cas13b in an inactive state[68].

Csx28 was only found in type VI-B2 systems and predicted to contain a transmembrane region and a divergent HEPN domain[33]. Csx28 might enhance the collateral activity of Cas13b to increase its interference activity[33]. A recent cryo-EM structure of *Pb*Csx28 revealed that it exists as an octamer, with the transmembrane region forming a positively charged pore (Fig. 6c)[69]. The predicted HEPN domains adopt a noncanonical arrangement and present a new topology of unknown function with no similarity to reported structures. Notably, the predicted key histidine and arginine residues in the R-$X_{4–6}$-H motif are located apart from each other and point in opposite directions and cannot form a catalytically competent composite nuclease pocket (zoomed-in box in Fig. 6c). Based on a combination of structural data and functional assays, it was proposed that Csx28 is activated by Cas13b, resulting in Csx28 pore formation and concomitant membrane depolarization[69]. Further assays are required to explore more details of the proposed hypothesis, specifically the nature of the trigger for activation as well as an understanding at the molecular level of the principle underlying membrane depolarization.

WYL domain-containing proteins contain a WYL domain and a helix–turn–helix or a ribbon–helix–helix DNA-binding domain[38]. The WYL domain-containing protein has been reported as a negative regulator of type I-D systems through transcriptional repression and is predicted to sense nucleic acids or nucleotide derivatives[70,71]. In subtype VI-D systems, *Ruminococcus* sp. *Rsp*WYL1 increases in vitro *cis*- and *trans*-RNase activities of *Rsp*Cas13d and its ortholog *Eubacterium siraeum* DSM 15702 (*Es*Cas13d) as well as *Rsp*Cas13d-mediated in vivo RNA knockdown, suggesting a distinct transcription-independent mechanism[38]. Biochemical and structural data revealed that *Rsp*WYL1 consists of three domains (NTD, WYL and C-terminal domain (CTD)) and forms a homodimer through interactions between the NTD–NTD and CTD–CTD domains (Fig. 6d)[72]. *Rsp*WYL1 binds to ssRNA through WYL and CTD domains but has weak binding affinity for Cas13d[72]. *Rsp*WYL1 may act as an RNA sponge by positioning more RNA into the Cas13d catalytic pocket and/or allosterically enhancing Cas13d activity by physical interactions. The exact modulation mechanism remains unclear.

Inhibition by Acr proteins

Recent studies have identified AcrVIA1 as an anti-CRISPR inhibitor for Cas13a and AcrVIB1 for Cas13b[56,73,74]. Among these Acrs, the prophage-encoded AcrVIA1 physically interacted with the *Lse*Cas13a–crRNA binary complex, thereby reducing the RNase activity and abolishing Cas13a-induced cell dormancy[56]. Structural and biochemical analysis of

the binary *Lse*Cas13a–crRNA (structure not shown) and the ternary *Lse*Cas13a–crRNA–AcrVIA1 complex (Fig. 6e,f) elucidated that AcrVIA1 is positioned along the crRNA-exposed face of Cas13a in the ternary complex, thereby forming intermolecular contacts with the NTD, helical-1, linker and HEPN-1 domains of Cas13a as well as the 3′ segment of the spacer. These data indicate that AcrVIA1 not only prevents target RNA access and base pairing with the spacer but in addition blocks the conformational changes required for nuclease activation, thereby retaining Cas13a in the inactive state. Notably, a single dose of AcrVIA1 delivered by an individual virion completely dismantles type VI-A CRISPR-mediated immunity[56], unlike inhibitors of DNA-cleaving Cas nucleases, which caused limited immunosuppression and require multiple infections to bypass CRISPR defenses. Additional research identifying a proposed subset of AcrVIA proteins that reduced Cas13a nuclease activity and prevented Cas13-mediated RNA targeting and editing in bacteria and human cells[73] has been challenged[75] and remains controversial.

Biotechnological applications based on active Cas13

Type VI systems engendered tremendous interest given that the Cas13–crRNA effector acts as a scaffold necessary for targeted cleavage of ssRNA, expanding the programmable manipulation of transcripts at the RNA level without heritable genome editing. There are opportunities for the application of active Cas13 in biotechnological applications ranging from programmable RNA knockdown to nucleic acid detection.

Programmable RNA knockdown or degradation

Cas13a, Cas13b, Cas13bt and Cas13d have been used for programmable RNA knockdown in prokaryotic and eukaryotic cells and animal models[34,36,44,62,63,76–82], in which RfxCas13d and Cas13bt mediated robust and either comparable or higher knockdown efficiency of the endogenous transcript[34,44]. Moreover, the size of Cas13d and Cas13bt is more compact than Cas13a–Cas13c, which provides potential advantages in adeno-associated virus (AAV)-mediated delivery.

Cas13-mediated RNA knockdowns have been explored for their therapeutic potential in repressing pathogen infection by degradation of pathogenic RNA. The elimination efficiency of viral and bacterial RNA was investigated in mammalian and plant cell lines and indicated that Cas13 could significantly reduce infection[79,83–89]. Further studies performed in animal models by the mRNA-encoded Cas13 approach suggested efficient reduction of influenza RNA in mice and mitigation of severe acute respiratory syndrome coronavirus 2 infection in hamsters[90].

*Lwa*Cas13a-, *Rfx*Cas13d- and *Psp*Cas13b-mediated off-target activities have been observed in *Drosophila*[91,92] and some human cell lines[93–95]. Structural-based mutation design has been used to engineer Cas13d and Cas13X with reduced off-target effects in human cell lines, mice and somatic cells[96]. Machine learning and deep learning as well as a large-scale Cas13d-based screening dataset have been used to systematically evaluate on-target activity and off-target effects. These efforts have permitted prediction of on-target activity of a crRNA[97,98], which sheds light on the systematic and comprehensive evaluation of the correlation between on- and off-target effects and different factors such as the expression

level of target RNA, cell types and target accessibility, among others. Some caution is needed in interpretation of the available literature given concerns about discrepancies based on different controls, inconsistent vectors, variable protein constructs and guide designs, which could result in inconsistent observation of how Cas13 behaves in a test tube, how it behaves in bacteria and how it behaves over varying cell types and make it very difficult to determine what drives on- and off-target activity.

Nucleic acid detection

Cas13 collateral *trans*-cleavage activity as monitored by fluorescent RNA has resulted in the development of emerging technologies for rapid, sensitive and specific nucleic acid detection in molecular diagnostics. Usually, the nucleic acid sample is amplified, which is then followed by transcription, thereby generating ssRNA targets (Fig. 7a). When the ssRNA target base pairs with the crRNA spacer, Cas13 is activated and *trans*-cleaves the fluorophore-quenched ssRNA reporter for fluorescence signal release (Fig. 7b). Isothermal amplification methods, which require lower temperature than traditional PCR amplification, have been integrated into Cas13-based detection applications for template amplification (Fig. 7a). The established methods, such as specific high-sensitivity enzymatic reporter unlocking (SHERLOCK), provide a limit of detection (LOD) at the attomolar level (~6.5 copies per μl)[99], which is comparable to that of reverse transcription–quantitative PCR (qRT–PCR), and furthermore have proved to be reliable in a clinical study[100–103]. Multiplexing using Cas13 and Cas12a orthologs in SHERLOCK enables multiplexed detection of four target sequences in one sample[104]. One way for sensitivity improvement involves incorporation with other protein components for signal amplification. A successful method, termed SHERLOCKv2, involves combination with the type III nuclease Csm6 and chemically modified ssRNA activators (Fig. 7c)[104,105]. Cas13 *trans*-cleaves the ssRNA activator to release activator cyclic oligoadenylates, which activate Csm6 RNase activity on the fluorophore-quenched ssRNA reporter and provide zeptomolar sensitivity[104,105]. Development of the amplification-free detection method with an LOD in the attomolar range is necessary for low concentration of DNA or RNA samples from clinical and environmental specimens. The fast integrated nuclease detection in tandem (FIND-IT) method uses the Cas13–Csm6 system and the combination of eight designed crRNA species to simultaneously target eight different positions of one single ssRNA, thereby allowing for an LOD of ~30 copies per μl without amplification[106]. Another approach involves protein engineering. By inserting the RNA-binding domain (RBD) into a loop region proximal to the active site of the HEPN domains, RBP-*Lwa*Cas13a variants achieve an LOD at the attomolar level without amplification[107]. Recent efforts have also been focused on optimizing reaction conditions[101], developing a field-deployable sample preparation platform[108] and integrating electrochemical microfluidic chips and sensors for quantitative and multiplexed signal readout[102,109–111]. Additional approaches for development of an amplification-free and ultra-sensitive detection method await development.

Biotechnological applications based on inactive Cas13

Catalytically inactive Cas13 (dCas13) can act as a programmable RNA-binding platform to bring modules close to the RNA of interest to change RNA characteristics, thereby

impacting on base editing, modification editing and splicing modulation or to study RNA localization and interaction with partner proteins.

RNA base editing

Site-specific RNA-based editing relies on the concept of dCas13-fused deaminase (Fig. 8a). By generating a single mismatch at the editing site, the flipped-out nucleotide is captured by deaminase. The first version of RNA base editor has been developed by fusing dCas13b with deaminase ADAR2 (adenosine deaminase acting on RNA type 2), termed REPAIR, and allows for adenosine-to-inosine (A-to-I) conversion[63,112]. The produced inosine mimics guanosine in translation and splicing reactions and achieves adenosine-to-guanosine exchange. One ADAR2 variant fused with Cas13b (named RESCUE), has served as a cytosine deaminase and has been used for cytosine-to-uridine (C-to-U) replacement[113]. However, the base editors REPAIR and RESCUE exhibited high off-target effects. The follow-up optimized methods, namely REPAIRv2 and RESCUE-S, showed reduced off-target rate following rational mutagenesis of ADAR2 (refs. 63,113). Later, other methods have been developed by fusing deaminases with other Cas13 orthologs including Cas13d and Cas13bt3 (also known as Cas13X.1), and these exhibited higher editing efficiency and/or lower off-target effects[44,78,114,115]. An ADAR2-dependent cytosine-to-uridine editor has retained activity on A-to-I conversion, resulting in off-target effects on adenosine. The cytidine deaminase APOBEC3A together with Cas13 exhibited higher efficiency than RESCUE-S[116].

Cas13 base editors allow nucleotide conversion on transcripts without changing DNA sequence, which provides an alternative approach toward site-direct RNA editing treatment for monogenic diseases. Several studies on the editing of pathogenic mutations in different cell types and mouse models have been reported and showed different efficiency in restoring protein expression[63,117–120]. As the editing systems have been established recently, a comprehensive evaluation of on-target activity and off-target effects on both RNA editing and related protein products still remains to be done.

Alternative splicing modulation

Alternative splicing of mRNA precursors (pre-mRNA) transcribed from a single gene produces diverse mRNA species that encode proteins with different sequences and activities, thereby increasing proteome diversity in different types of eukaryotic cells. Alternative splicing is modulated by the core splicing spliceosome machinery together with many RNA-binding proteins and regulatory splicing factors. These include serine/arginine-rich (SR) proteins belonging to the RNA recognition motif-containing SR family and SR-related proteins containing one or more S/R-rich low-complexity domains (RS domains)[121,122]. dCas13 has been applied for programmable control of alternative splicing using several strategies. By binding with splicing elements of target pre-mRNA, dCas13 alone can alter splicing and attempt to induce exon exclusion[34]. Given that this approach failed to induce exon inclusion, replacement of the RNA recognition motif of splicing factors with CasRx (named CASFx) enabled programmable control of alternative splicing[123] (Fig. 8b). When coupled with the chemical-inducible FKBP (FK506 binding protein)–FRB (FKBP–rapamycin binding) domain (named iCASFx), CASFx comes under the control of a

small molecule and allows for spatiotemporal control of alternative splicing. Subsequently optimized CASFx–SR, that is, derived from CASFx by fusing with RS domains, was able to manipulate alternative splicing and regulate SF expression, which acts as a convenient tool for evaluating the functional roles of splicing factors in tumors[124]. These methods provide a potential therapeutic solution for RNA mis-splicing diseases.

Programmable RNA m^{6}A modification

The formation, removal and function of N^6-methyladenosine (m^{6}A) modifications are regulated by a series of proteins: the methyltransferase complex METTL3–METTL14 and associated proteins, demethylases FTO and ALKBH5 and readers YTHDF1–YTHDF3. dCas13 can be used as an adaptor for programmable RNA m^{6}A modification editing by fusing with different proteins, allowing investigation on the functional role of m^{6}A modification at single transcripts of interest in live cells[125] (Fig. 8c). Linking with methyltransferases or demethylases can be used to edit the status of m^{6}A modification at a single site in varied regions such the 3′-untranslated region (UTR) and the 5′-UTR in different cell localization conditions (nucleus or cytoplasm) with limited off-target effects[126–131]. Coupling with the m^{6}A readers YTHDF1 and YTHDF2 uncovered their functions in translation promotion and RNA degradation, respectively[132]. Two methods have been developed for m^{6}A modification editing at multiple sites or transcripts. The dCas13–FTO system with its CRISPR array can simultaneously target multiple sites[131]. Another method called targeted RNA demethylation by SunTag system (TRADES) uses dCas13 and the SunTag system[133]. The SunTag system is composed of the single-chain variable fragment (scFv) and multiple copies of its repeating-epitope GCN4 (an eukaryotic transcriptional activator protein) peptides, which are fused to a demethylase and dCas13 separately. Cas13–GCN4 recruits multiples of scFV–demethylases and achieves multiplexed m^{6}A editing. To achieve spatiotemporal control of site-specific m^{6}A modification editing, the blue light-sensitive protein CBIN and its adaptor CY2 were fused with dCas13 and methyltransferase or demethylase separately for the recruitment of each other under control of blue light[134]. dCas13-based m^{6}A editing tools may be applied in controlling disease progress by customized modifications in transcripts from oncogenes and tumor-suppressor genes. Ongoing research on programmable control of other RNA modifications such as m^{1}A and m^{5}C is being undertaken by fusing dCas13 with the respective methylases, demethylases and readers.

RNA imaging in live cells

dCas13 enables endogenous RNA visualization in live cells by coupling with fluorescent proteins or split fluorophores. The most straightforward method is to use fluorescence-labeled dCas13 for detection of endogenous RNA transcripts[62] (Fig. 8d). Other methods such as SunTag and split fluorophores have been used to increase fluorescence signal and reduce background noise. By fusing multiple copies of the GCN4 peptide and scFv with Cas13 and fluorescence protein separately, the SunTag system can amplify the fluorescence signal[135]. Furthermore, split fluorophores together with the Cas13a–SunTag system produced a better signal-to-noise ratio than that of the previously established the MS2 and MS2-coat protein (MS2–MCP) system[136]. Despite the preponderance of single-transcript imaging, coupling dCas13 orthologs with different fluorescent proteins

can provide simultaneous two-transcript imaging in single cells. Moreover, combination of dCas13 with the MS2–MCP or dCas9 system enables dual-color imaging of two different transcripts or alternately RNA transcripts and genomic DNA, respectively[137–139]. Current Cas13-based RNA imaging approaches expand our understanding of nuclear activities but still show limitation for low-abundance transcripts or RNA with secondary structures. Therefore, a versatile multiple-color image toolkit with low background noise needs to be established.

Mapping RNA–protein interactions

dCas13 could be applied to identify proteins interacting with RNA of interest in live cells. These approaches rely on the binding of dCas13 to target specific RNA and in the process capturing surrounding related RNA-binding proteins by UV cross-linking proteins physically bound to Cas13 (named CBRIP)[140] or proximity labeling proteins with biotin by enzymes including ligase and ascorbate peroxidase (Fig. 8e). dCas13 fused to the ligase PafA (named CRUIS) can mediate ligation of surrounding proteins with biotin-tagged PupE[141]. Similarly, the dCas13-fused ligase BASU (named CARPID) allows for biotinylating adjacent proteins. The dCas13-fused peroxidase APEX2 has been applied to biotinylate proteins within a distance of 25 nm with the addition with H_2O_2 and biotin-phenol[142]. To improve efficiency, a double-stranded RBD from human protein kinase R (PKR) was fused to the C terminus of dCas13, which stabilizes the RNA duplex and exhibits an increased enrichment level of proteins. However, these methods have limitations related to low abundance of targeted RNA and transient and unstable RNA–protein interactions.

Translational regulation

As active Cas13 showed toxicity and induced cell dormancy in bacteria due to its collateral activities[36,65], dCas13 has been repurposed for translational repression without affecting mRNA stability (Fig. 8f). dCas13d can be programmed to tightly bind with target mRNA and act as a road blocker to prevent ribosome binding or movement, thereby resulting in translational repression (Fig. 8f, top left). Engineered dCas13-based translational repression platforms have been established by targeting ribosomal binding sites or the 5′ end of the open reading frame and exhibited effective translational repression in cell-free expression systems[143] and in *E. coli* cells[144]. The dCas13-based strategy (named CRISPRδ) has also been used to repress translation in human HEK293 cells by targeting the 5′-UTR or the start codon[145]. By screening different translational repressor proteins, further enhancement of the repression effects can be achieved using the dCas13–4EHP (eIF4E-homologous protein, also termed eIF4E2) fusion protein and allows for expanded targeting sites including the start codon, the 5′-UTR and the 3′-UTR[145] (Fig. 8f, bottom left). Additionally, dCas13 can also be used to activate translation initiation of a fluorescent protein encoded by *cis*-repressed mRNA in a cell-free expression system and in *E. coli* cells[143]. dCas13 fused with the translation initiation factor IF3 provided significant enhanced expression of fluorescent protein and a native gene encoding β-galactosidase in *E. coli* cells[146] (Fig. 8f, top right). In an alternative dCasRx-based approach, crRNA was covalently linked with the SINEB2 (short non-pairing interspersed nuclear element (SINE) B2) element of the long noncoding RNA uchl1, enabling increased expression of fluorescent protein in several cell lines and endogenous tumor-suppressor proteins in bladder cancer cells, respectively[147] (Fig. 8f,

bottom right). These strategies provide potent and efficient tools for translational regulation regardless of mRNA degradation.

Future challenges

Compared to the Cas9 and Cas12 systems, RNA-guided Cas13 systems intrinsically target RNA instead of DNA, giving more benefit to on-target specificity. Importantly, recently discovered type III-E systems elegantly deploy the single Cas protein gRAMP (also known as Cas7–11) for ssRNA cleavage and are associated with caspase-like TPR-CHAT (also known as Csx29) for potential protein targeting[94,148]. Space limitations do not allow us to describe this interesting system. In addition, the relatively compact type V-G Cas12g displays RNA-guided cleavage activity on target ssRNA and collateral RNase and DNase activities[149]. Compared with type VI Cas13 systems, these two types are evolutionarily distant, structurally unrelated and rely on distinctly different mechanisms for not only pre-crRNA processing but also sensing and cleavage of target RNA, which expands the toolbox for RNA manipulation tools. Given the simplicity of composition and diverse RNA-centric target properties, Cas13 has attracted attention as a promising RNA detection and manipulation platform.

Other type VI Cas13 subtypes

To date, only the assembly and RNA recognition mechanisms of subtypes VI-A and VI-D have been investigated in depth, leaving a number of challenges that need to be addressed in the future. Thus, (1) whether target RNA and substrate RNA access the catalytic pocket in the same manner among different subtypes remains unknown. (2) How orthologs such as Cas13b and Cas13c scan and load target RNA is still unclear. (3) The pathway to prevent autoimmunity in other subtypes except VI-A remains to be determined. (4) The accurate modulation mechanisms of Acr proteins and intrinsic accessory proteins targeting type VI systems remain to be explored. In the future, we anticipate expansion of new subtypes with new functional features through the screening of ever-growing genomic and metagenomic databases, with the capacity for identification and development of new systems harboring advantageous properties.

Effect of off-target effects

The major concern of currently available Cas13-based RNA-targeting technologies is the complication associated with widespread off-target effects. Both wild-type and dCas13-based technologies such as knockdown or base editors exhibit off-target effects. Thus, minimization of off-target effects remains a major challenge that needs to be overcome for effective clinical applications of this methodology.

Cellular delivery of Cas13–RNA

A second concern relates to effective all-in-one AAV delivery of a CRISPR array or guide RNA, an engineered Cas13 encoding gene, an optional module and required expression or regulatory elements. The development of a smaller, more efficient and less cytotoxic Cas13 toolkit will be of great importance for manipulation of primary cells and clinical treatments.

Recent advances associated with the remarkably small size of Cas13bt, Cas13ct and Cas13d should encourage further development of engineered small Cas13 effectors.

Effect of immunogenic and cytotoxic effects

A further concern relates to the potential immunogenic and cytotoxic effects of Cas13. Surprisingly, crRNA alone substantially reduced viral RNA expression and presented stronger suppression on addition of *Psp*Cas13b in insect cells, which has not been observed in mammalian and plant cells[150]. It remains unclear whether other Cas13 proteins alone or bound to their cognate crRNA cause similar cell growth repression in insect or other eukaryotic cells.

Benefits of Cas13-based therapeutic intervention

Before the development of CRISPR-based technologies, antisense oligonucleotides and RNA interference approaches were effective for RNA knockdown and have been clinically used for RNA-targeting therapies even often with off-target effects. Cas13 systems have exhibited high efficiency and specificity in RNA knockdown in mouse disease models. Importantly, Cas13-based strategies have also expanded beyond knockdown capacities, allowing for base editing, RNA demethylation, splicing modulation and translational regulation. These valuable Cas13-based approaches can be achieved through delivery from AAV vectors, providing strong candidates for future durable RNA-targeting therapies.

Supplementary Material

Refer to Web version on PubMed Central for supplementary material.

Acknowledgements

H.Y. was supported by grants from the CAS project for Young Scientists in Basic research (YSBR-009), the Strategic Priority Research Program of the Chinese Academy of Science (XDB0570300), the National Key R&D Program of China (2023YFA0915600), the Natural Science Foundation of China (32171266 and 31971135), the Shanghai Rising-Star Program (20QA1410700) and the National Natural Science Foundation of Shanghai (22ZR1468900). D.J.P. was supported by funds from the NIH (GM129430, GM145888 and AI141507), the Maloris Foundation and Memorial Sloan-Kettering Cancer Center Core grant P30 CA008748.

References

1. Jia N & Patel DJ Structure-based functional mechanisms and biotechnology applications of anti-CRISPR proteins. Nat. Rev. Mol. Cell Biol. 22, 563–579 (2021). [PubMed: 34089013]
2. Borges AL, Davidson AR & Bondy-Denomy J The discovery, mechanisms, and evolutionary impact of anti-CRISPRs. Annu. Rev. Virol. 4, 37–59 (2017). [PubMed: 28749735]
3. Davidson AR et al. Anti-CRISPRs: protein inhibitors of CRISPR–Cas systems. Annu. Rev. Biochem. 89, 309–332 (2020). [PubMed: 32186918]
4. Li Y & Bondy-Denomy J Anti-CRISPRs go viral: the infection biology of CRISPR–Cas inhibitors. Cell Host Microbe 29, 704–714 (2021). [PubMed: 33444542]
5. Pawluk A, Davidson AR & Maxwell KL Anti-CRISPR: discovery, mechanism and function. Nat. Rev. Microbiol. 16, 12–17 (2018). [PubMed: 29062071]
6. Shivram H, Cress BF, Knott GJ & Doudna JA Controlling and enhancing CRISPR systems. Nat. Chem. Biol. 17, 10–19 (2021). [PubMed: 33328654]
7. Sontheimer EJ & Davidson AR Inhibition of CRISPR–Cas systems by mobile genetic elements. Curr. Opin. Microbiol. 37, 120–127 (2017). [PubMed: 28668720]

8. Stanley SY & Maxwell KL Phage-encoded anti-CRISPR defenses. Annu. Rev. Genet. 52, 445–464 (2018). [PubMed: 30208287]
9. Trasanidou D et al. Keeping CRISPR in check: diverse mechanisms of phage-encoded anti-CRISPRs. FEMS Microbiol. Lett. 366, fnz098 (2019). [PubMed: 31077304]
10. Wiegand T, Karambelkar S, Bondy-Denomy J & Wiedenheft B Structures and strategies of anti-CRISPR-mediated immune suppression. Annu. Rev. Microbiol. 74, 21–37 (2020). [PubMed: 32503371]
11. Marino ND, Pinilla-Redondo R, Csorgo B & Bondy-Denomy J Anti-CRISPR protein applications: natural brakes for CRISPR–Cas technologies. Nat. Methods 17, 471–479 (2020). [PubMed: 32203383]
12. van der Oost J, Westra ER, Jackson RN & Wiedenheft B Unravelling the structural and mechanistic basis of CRISPR–Cas systems. Nat. Rev. Microbiol. 12, 479–492 (2014). [PubMed: 24909109]
13. Jackson RN, van Erp PB, Sternberg SH & Wiedenheft B Conformational regulation of CRISPR-associated nucleases. Curr. Opin. Microbiol. 37, 110–119 (2017). [PubMed: 28646675]
14. Nishimasu H & Nureki O Structures and mechanisms of CRISPR RNA-guided effector nucleases. Curr. Opin. Struct. Biol. 43, 68–78 (2017). [PubMed: 27912110]
15. Molina R, Sofos N & Montoya G Structural basis of CRISPR–Cas type III prokaryotic defence systems. Curr. Opin. Struct. Biol. 65, 119–129 (2020). [PubMed: 32712502]
16. Nussenzweig PM & Marraffini LA Molecular mechanisms of CRISPR–Cas immunity in bacteria. Annu. Rev. Genet. 54, 93–120 (2020). [PubMed: 32857635]
17. Koonin EV & Makarova KS Evolutionary plasticity and functional versatility of CRISPR systems. PLoS Biol. 20, e3001481 (2022). [PubMed: 34986140]
18. McGinn J & Marraffini LA Molecular mechanisms of CRISPR–Cas spacer acquisition. Nat. Rev. Microbiol. 17, 7–12 (2019). [PubMed: 30171202]
19. Koonin EV, Makarova KS & Zhang F Diversity, classification and evolution of CRISPR–Cas systems. Curr. Opin. Microbiol. 37, 67–78 (2017). [PubMed: 28605718]
20. Amitai G & Sorek R CRISPR–Cas adaptation: insights into the mechanism of action. Nat. Rev. Microbiol. 14, 67–76 (2016). [PubMed: 26751509]
21. Mosterd C, Rousseau GM & Moineau S A short overview of the CRISPR–Cas adaptation stage. Can. J. Microbiol. 67, 1–12 (2021). [PubMed: 32559396]
22. Sasnauskas G & Siksnys V CRISPR adaptation from a structural perspective. Curr. Opin. Struct. Biol. 65, 17–25 (2020). [PubMed: 32570107]
23. Hochstrasser ML & Doudna JA Cutting it close: CRISPR-associated endoribonuclease structure and function. Trends Biochem. Sci. 40, 58–66 (2015). [PubMed: 25468820]
24. Deltcheva E et al. CRISPR RNA maturation by *trans*-encoded small RNA and host factor RNase III. Nature 471, 602–607 (2011). [PubMed: 21455174]
25. Brouns SJ et al. Small CRISPR RNAs guide antiviral defense in prokaryotes. Science 321, 960–964 (2008). [PubMed: 18703739]
26. Wiedenheft B, Sternberg SH & Doudna JA RNA-guided genetic silencing systems in bacteria and archaea. Nature 482, 331–338 (2012). [PubMed: 22337052]
27. Marraffini LA & Sontheimer EJ CRISPR interference: RNA-directed adaptive immunity in bacteria and archaea. Nat. Rev. Genet. 11, 181–190 (2010). [PubMed: 20125085]
28. Garneau JE et al. The CRISPR/Cas bacterial immune system cleaves bacteriophage and plasmid DNA. Nature 468, 67–71 (2010). [PubMed: 21048762]
29. Makarova KS et al. Evolution and classification of the CRISPR–Cas systems. Nat. Rev. Microbiol. 9, 467–477 (2011). [PubMed: 21552286]
30. Makarova KS, Zhang F & Koonin EV SnapShot: class 1 CRISPR–Cas systems. Cell 168, 946 (2017). [PubMed: 28235204]
31. Makarova KS, Zhang F & Koonin EV SnapShot: class 2 CRISPR–Cas systems. Cell 168, 328 (2017). [PubMed: 28086097]
32. Shmakov S et al. Diversity and evolution of class 2 CRISPR–Cas systems. Nat. Rev. Microbiol. 15, 169–182 (2017). [PubMed: 28111461]

33. Smargon AA et al. Cas13b is a type VI-B CRISPR-associated RNA-guided RNase differentially regulated by accessory proteins Csx27 and Csx28. Mol. Cell 65, 618–630 (2017). [PubMed: 28065598]
34. Konermann S et al. Transcriptome engineering with RNA-targeting type VI-D CRISPR effectors. Cell 173, 665–676 (2018). [PubMed: 29551272]
35. Meeske AJ, Nakandakari-Higa S & Marraffini LA Cas13-induced cellular dormancy prevents the rise of CRISPR-resistant bacteriophage. Nature 570, 241–245 (2019). [PubMed: 31142834] The paper demonstrates that the trans-RNase activity of Cas13 arrests host growth, thereby interrupting the infectious cycle.
36. Abudayyeh OO et al. C2c2 is a single-component programmable RNA-guided RNA-targeting CRISPR effector. Science 353, aaf5573 (2016). [PubMed: 27256883] This article characterizes Cas13 (known as C2c2) for the first time and shows that Cas13a can be programmed for RNA interference in E. coli cells.
37. van Beljouw SPB, Sanders J, Rodriguez-Molina A & Brouns SJJ RNA-targeting CRISPR–Cas systems. Nat. Rev. Microbiol. 21, 21–34 (2023). [PubMed: 36171275]
38. Yan WX et al. Cas13d is a compact RNA-targeting type VI CRISPR effector positively modulated by a WYL-domain-containing accessory protein. Mol. Cell 70, 327–339 (2018). [PubMed: 29551514]
39. Smargon AA, Shi YJ & Yeo GW RNA-targeting CRISPR systems from metagenomic discovery to transcriptomic engineering. Nat. Cell Biol. 22, 143–150 (2020). [PubMed: 32015437]
40. Terns MP CRISPR-based technologies: impact of RNA-targeting systems. Mol. Cell 72, 404–412 (2018). [PubMed: 30388409]
41. Knott GJ & Doudna JA CRISPR–Cas guides the future of genetic engineering. Science 361, 866–869 (2018). [PubMed: 30166482]
42. Pickar-Oliver A & Gersbach CA The next generation of CRISPR–Cas technologies and applications. Nat. Rev. Mol. Cell Biol. 20, 490–507 (2019). [PubMed: 31147612]
43. Wang JY, Pausch P & Doudna JA Structural biology of CRISPR–Cas immunity and genome editing enzymes. Nat. Rev. Microbiol. 20, 641–656 (2022). [PubMed: 35562427]
44. Xu C et al. Programmable RNA editing with compact CRISPR–Cas13 systems from uncultivated microbes. Nat. Methods 18, 499–506 (2021). [PubMed: 33941935] Together with ref. [45], this paper reports the smallest known Cas13 orthologs and demonstrates their utility as RNA editors.
45. Kannan S et al. Compact RNA editors with small Cas13 proteins. Nat. Biotechnol. 40, 194–197 (2022). [PubMed: 34462587] Together with ref. [44], this paper reports the smallest known Cas13 orthologs and demonstrates their utility as RNA editors.
46. Shmakov S et al. Discovery and functional characterization of diverse class 2 CRISPR–Cas systems. Mol. Cell 60, 385–397 (2015). [PubMed: 26593719] This paper provides the first computational pipeline to search for uncharacterized CRISPR–Cas loci by using cas1 as the seed.
47. Hoikkala V et al. Cooperation between different CRISPR–Cas types enables adaptation in an RNA-targeting system. mBio 12, e03338–20 (2021). [PubMed: 33785624]
48. O'Connell MR Molecular mechanisms of RNA targeting by Cas13-containing type VI CRISPR–Cas systems. J. Mol. Biol. 431, 66–87 (2019). [PubMed: 29940185]
49. Perculija V, Lin J, Zhang B & Ouyang S Functional features and current applications of the RNA-targeting type VI CRISPR–Cas systems. Adv. Sci. 8, 2004685 (2021).
50. East-Seletsky A et al. Two distinct RNase activities of CRISPR–C2c2 enable guide-RNA processing and RNA detection. Nature 538, 270–273 (2016). [PubMed: 27669025]
51. Zhang C et al. Structural basis for the RNA-guided ribonuclease activity of CRISPR–Cas13d. Cell 175, 212–223 (2018). [PubMed: 30241607]
52. Knott GJ et al. Guide-bound structures of an RNA-targeting A-cleaving CRISPR–Cas13a enzyme. Nat. Struct. Mol. Biol. 24, 825–833 (2017). [PubMed: 28892041]
53. East-Seletsky A, O'Connell MR, Burstein D, Knott GJ & Doudna JA RNA targeting by functionally orthogonal type VI-A CRISPR–Cas enzymes. Mol. Cell 66, 373–383 (2017). [PubMed: 28475872]
54. Liu L et al. Two distant catalytic sites are responsible for C2c2 RNase activities. Cell 168, 121–134 (2017). [PubMed: 28086085]

55. Liu L et al. The molecular architecture for RNA-guided RNA cleavage by Cas13a. Cell 170, 714–726 (2017). [PubMed: 28757251] The two papers (refs. [54,55]) conducted by Liu et al. report the first structures of Cas13a in apo, crRNA-bound and target RNA-bound states, thereby providing mechanistic insights into how Cas13a functions.
56. Meeske AJ et al. A phage-encoded anti-CRISPR enables complete evasion of type VI-A CRISPR–Cas immunity. Science 369, 54–59 (2020). [PubMed: 32467331] This article provides the first detailed mechanistic insights into an Acr targeting Cas13 systems, which is associated with complete evasion of Cas13-mediated immunity.
57. Kick LM, von Wrisberg MK, Runtsch LS & Schneider S Structure and mechanism of the RNA dependent RNase Cas13a from Rhodobacter capsulatus. Commun. Biol. 5, 71 (2022). [PubMed: 35058543]
58. Slaymaker IM et al. High-resolution structure of Cas13b and biochemical characterization of RNA targeting and cleavage. Cell Rep. 26, 3741–3751 (2019). [PubMed: 30917325]
59. Zhang B et al. Structural insights into Cas13b-guided CRISPR RNA maturation and recognition. Cell Res. 28, 1198–1201 (2018). [PubMed: 30425321]
60. Zhang B et al. Two HEPN domains dictate CRISPR RNA maturation and target cleavage in Cas13d. Nat. Commun. 10, 2544 (2019). [PubMed: 31186424]
61. Tambe A, East-Seletsky A, Knott GJ, Doudna JA & O'Connell MR RNA binding and HEPN-nuclease activation are decoupled in CRISPR–Cas13a. Cell Rep. 24, 1025–1036 (2018). [PubMed: 30044970]
62. Abudayyeh OO et al. RNA targeting with CRISPR–Cas13. Nature 550, 280–284 (2017). [PubMed: 28976959] This article reports Cas13-based RNA knockdown and binding platforms in mammalian cells.
63. Cox DBT et al. RNA editing with CRISPR–Cas13. Science 358, 1019–1027 (2017). [PubMed: 29070703] This article reports a Cas13-based RNA A-to-I editing system in mammalian cells.
64. Tong H & Yang H Engineered Cas13 variants with minimal collateral RNA targeting. Nat. Biotechnol. 41, 29–30 (2023). [PubMed: 35962198]
65. Jain I et al. tRNA anticodon cleavage by target-activated CRISPR–Cas13a effector. Preprint at bioRxiv 10.1101/2021.11.10.468108 (2021).
66. Meeske AJ & Marraffini LA RNA guide complementarity prevents self-targeting in type VI CRISPR systems. Mol. Cell 71, 791–801 (2018). [PubMed: 30122537]
67. Wang B et al. Structural basis for self-cleavage prevention by tag:anti-tag pairing complementarity in type VI Cas13 CRISPR systems. Mol. Cell 81, 1100–1115 (2021). [PubMed: 33472057]
68. Makarova KS, Gao L, Zhang F & Koonin EV Unexpected connections between type VI-B CRISPR–Cas systems, bacterial natural competence, ubiquitin signaling network and DNA modification through a distinct family of membrane proteins. FEMS Microbiol. Lett. 366, fnz088 (2019). [PubMed: 31089700]
69. VanderWal AR et al. Csx28 is a membrane pore that enhances CRISPR–Cas13b-dependent antiphage defense. Science 380, 410–415 (2023). [PubMed: 37104586]
70. Makarova KS, Anantharaman V, Grishin NV, Koonin EV & Aravind L CARF and WYL domains: ligand-binding regulators of prokaryotic defense systems. Front. Genet. 5, 102 (2014). [PubMed: 24817877]
71. Hein S, Scholz I, Voss B & Hess WR Adaptation and modification of three CRISPR loci in two closely related cyanobacteria. RNA Biol. 10, 852–864 (2013). [PubMed: 23535141]
72. Zhang H, Dong C, Li L, Wasney GA & Min J Structural insights into the modulatory role of the accessory protein WYL1 in the type VI-D CRISPR–Cas system. Nucleic Acids Res. 47, 5420–5428 (2019). [PubMed: 30976796]
73. Lin P et al. CRISPR–Cas13 inhibitors block RNA editing in bacteria and mammalian cells. Mol. Cell 78, 850–861 (2020). [PubMed: 32348779]
74. Wandera KG et al. Anti-CRISPR prediction using deep learning reveals an inhibitor of Cas13b nucleases. Mol. Cell 82, 2714–2726 (2022). [PubMed: 35649413]
75. Johnson MC, Hille LT, Kleinstiver BP, Meeske AJ & Bondy-Denomy J Lack of Cas13a inhibition by anti-CRISPR proteins from *Leptotrichia* prophages. Mol. Cell 82, 2161–2166 (2022). [PubMed: 35623354]

76. Jing X et al. Implementation of the CRISPR–Cas13a system in fission yeast and its repurposing for precise RNA editing. Nucleic Acids Res. 46, e90 (2018). [PubMed: 29860393]
77. Huynh N, Depner N, Larson R & King-Jones K A versatile toolkit for CRISPR–Cas13-based RNA manipulation in *Drosophila*. Genome Biol. 21, 279 (2020). [PubMed: 33203452]
78. Kannan S et al. Compact RNA editors with small Cas13 proteins. Nat. Biotechnol. 40, 194–197 (2021). [PubMed: 34462587]
79. Aman R et al. RNA virus interference via CRISPR/Cas13a system in plants. Genome Biol. 19, 1 (2018). [PubMed: 29301551]
80. Kushawah G et al. CRISPR–Cas13d induces efficient mRNA knockdown in animal embryos. Dev. Cell 54, 805–817 (2020). [PubMed: 32768421]
81. Li S et al. Screening for functional circular RNAs using the CRISPR–Cas13 system. Nat. Methods 18, 51–59 (2021). [PubMed: 33288960]
82. Zhang Y et al. Optimized RNA-targeting CRISPR/Cas13d technology outperforms shRNA in identifying functional circRNAs. Genome Biol. 22, 41 (2021). [PubMed: 33478577]
83. Bawage SS, Tiwari PM & Santangelo PJ Synthetic mRNA expressed Cas13a mitigates RNA virus infections. Preprint at *bioRxiv* 10.1101/370460 (2018).
84. Abbott TR et al. Development of CRISPR as an antiviral strategy to combat SARS-CoV-2 and influenza. Cell 181, 865–876 (2020). [PubMed: 32353252]
85. Cui J, Techakriengkrai N, Nedumpun T & Suradhat S Abrogation of PRRSV infectivity by CRISPR–Cas13b-mediated viral RNA cleavage in mammalian cells. Sci. Rep. 10, 9617 (2020). [PubMed: 32541822]
86. Fareh M et al. Reprogrammed CRISPR–Cas13b suppresses SARS-CoV-2 replication and circumvents its mutational escape through mismatch tolerance. Nat. Commun. 12, 4270 (2021). [PubMed: 34257311]
87. Aman R, Mahas A, Butt H, Aljedaani F & Mahfouz M Engineering RNA virus interference via the CRISPR/Cas13 machinery in Arabidopsis. Viruses 10, 732 (2018). [PubMed: 30572690]
88. Freije CA et al. Programmable inhibition and detection of RNA viruses using Cas13. Mol. Cell 76, 826–837 (2019). [PubMed: 31607545]
89. Kiga K et al. Development of CRISPR–Cas13a-based antimicrobials capable of sequence-specific killing of target bacteria. Nat. Commun. 11, 2934 (2020). [PubMed: 32523110]
90. Blanchard EL et al. Treatment of influenza and SARS-CoV-2 infections via mRNA-encoded Cas13a in rodents. Nat. Biotechnol. 39, 717–726 (2021). [PubMed: 33536629]
91. Buchman AB et al. Programmable RNA targeting using CasRx in flies. CRISPR J. 3, 164–176 (2020). [PubMed: 32584145]
92. Ai Y, Liang D & Wilusz JE CRISPR/Cas13 effectors have differing extents of off-target effects that limit their utility in eukaryotic cells. Nucleic Acids Res. 50, e65 (2022). [PubMed: 35244715]
93. Wang Q et al. The CRISPR–Cas13a gene-editing system induces collateral cleavage of RNA in glioma cells. Adv. Sci. 6, 1901299 (2019).
94. Ozcan A et al. Programmable RNA targeting with the single-protein CRISPR effector Cas7–11. Nature 597, 720–725 (2021). [PubMed: 34489594]
95. Wang L, Zhou J, Wang Q, Wang Y & Kang C Rapid design and development of CRISPR–Cas13a targeting SARS-CoV-2 spike protein. Theranostics 11, 649–664 (2021). [PubMed: 33391497]
96. Tong H et al. High-fidelity Cas13 variants for targeted RNA degradation with minimal collateral effects. Nat. Biotechnol. 41, 108–119 (2023). [PubMed: 35953673]
97. Wessels HH et al. Massively parallel Cas13 screens reveal principles for guide RNA design. Nat. Biotechnol. 38, 722–727 (2020). [PubMed: 32518401]
98. Cheng X et al. Modeling CRISPR–Cas13d on-target and off-target effects using machine learning approaches. Nat. Commun. 14, 752 (2023). [PubMed: 36765063]
99. Gootenberg JS et al. Nucleic acid detection with CRISPR–Cas13a/C2c2. Science 356, 438–442 (2017). [PubMed: 28408723]
100. Patchsung M et al. Clinical validation of a Cas13-based assay for the detection of SARS-CoV-2 RNA. Nat. Biomed. Eng. 4, 1140–1149 (2020). [PubMed: 32848209]

101. Arizti-Sanz J et al. Streamlined inactivation, amplification, and Cas13-based detection of SARS-CoV-2. Nat. Commun. 11, 5921 (2020). [PubMed: 33219225]
102. Fozouni P et al. Amplification-free detection of SARS-CoV-2 with CRISPR–Cas13a and mobile phone microscopy. Cell 184, 323–333 (2021). [PubMed: 33306959]
103. Joung J et al. Detection of SARS-CoV-2 with SHERLOCK one-pot testing. N. Engl. J. Med. 383, 1492–1494 (2020). [PubMed: 32937062]
104. Gootenberg JS et al. Multiplexed and portable nucleic acid detection platform with Cas13, Cas12a, and Csm6. Science 360, 439–444 (2018). [PubMed: 29449508]
105. Kellner MJ, Koob JG, Gootenberg JS, Abudayyeh OO & Zhang F SHERLOCK: nucleic acid detection with CRISPR nucleases. Nat. Protoc. 14, 2986–3012 (2019). [PubMed: 31548639]
106. Liu TY et al. Accelerated RNA detection using tandem CRISPR nucleases. Nat. Chem. Biol. 17, 982–988 (2021). [PubMed: 34354262]
107. Yang J et al. Engineered LwaCas13a with enhanced collateral activity for nucleic acid detection. Nat. Chem. Biol. 19, 45–54 (2023). [PubMed: 36138140]
108. Myhrvold C et al. Field-deployable viral diagnostics using CRISPR–Cas13. Science 360, 444–448 (2018). [PubMed: 29700266]
109. Qin P et al. Rapid and fully microfluidic Ebola virus detection with CRISPR–Cas13a. ACS Sens. 4, 1048–1054 (2019). [PubMed: 30860365]
110. Ackerman CM et al. Massively multiplexed nucleic acid detection with Cas13. Nature 582, 277–282 (2020). [PubMed: 32349121]
111. Bruch R et al. CRISPR/Cas13a-powered electrochemical microfluidic biosensor for nucleic acid amplification-free miRNA diagnostics. Adv. Mater. 31, e1905311 (2019). [PubMed: 31663165]
112. Tan MH et al. Dynamic landscape and regulation of RNA editing in mammals. Nature 550, 249–254 (2017). [PubMed: 29022589]
113. Abudayyeh OO et al. A cytosine deaminase for programmable single-base RNA editing. Science 365, 382–386 (2019). [PubMed: 31296651]
114. Liu Y et al. REPAIRx, a specific yet highly efficient programmable A > I RNA base editor. EMBO J. 39, e104748 (2020). [PubMed: 33058207]
115. Li G et al. Developing PspCas13b-based enhanced RESCUE system, eRESCUE, with efficient RNA base editing. Cell Commun. Signal. 19, 84 (2021). [PubMed: 34380502]
116. Huang X et al. Programmable C-to-U RNA editing using the human APOBEC3A deaminase. EMBO J. 39, e104741 (2020). [PubMed: 33058229]
117. Fry LE, Peddle CF, Barnard AR, McClements ME & MacLaren RE RNA editing as a therapeutic approach for retinal gene therapy requiring long coding sequences. Int. J. Mol. Sci. 21, 777 (2020). [PubMed: 31991730]
118. Rashnonejad A, Amini-Chermahini G, Taylor NK, Wein N & Harper SQ Designed U7 snRNAs inhibit *DUX4* expression and improve FSHD-associated outcomes in *DUX4* overexpressing cells and FSHD patient myotubes. Mol. Ther. Nucleic Acids 23, 476–486 (2021). [PubMed: 33510937]
119. Xiao Q et al. Rescue of autosomal dominant hearing loss by in vivo delivery of mini dCas13X-derived RNA base editor. Sci. Transl. Med. 14, eabn0449 (2022). [PubMed: 35857824]
120. Melfi R et al. Investigating REPAIRv2 as a tool to edit CFTR mRNA with premature stop codons. Int. J. Mol. Sci. 21, 4781 (2020). [PubMed: 32640650]
121. Manning KS & Cooper TA The roles of RNA processing in translating genotype to phenotype. Nat. Rev. Mol. Cell Biol. 18, 102–114 (2017). [PubMed: 27847391]
122. Dvinge H, Kim E, Abdel-Wahab O & Bradley RK RNA splicing factors as oncoproteins and tumour suppressors. Nat. Rev. Cancer 16, 413–430 (2016). [PubMed: 27282250]
123. Du M, Jillette N, Zhu JJ, Li S & Cheng AW CRISPR artificial splicing factors. Nat. Commun. 11, 2973 (2020). [PubMed: 32532987]
124. Leclair NK et al. Poison exon splicing regulates a coordinated network of SR protein expression during differentiation and tumorigenesis. Mol. Cell 80, 648–665 (2020). [PubMed: 33176162]
125. Rauch S et al. Programmable RNA-guided RNA effector proteins built from human parts. Cell 178, 122–134 (2019). [PubMed: 31230714]

126. Xia Z et al. Epitranscriptomic editing of the RNA N^6-methyladenosine modification by dCasRx conjugated methyltransferase and demethylase. Nucleic Acids Res. 49, 7361–7374 (2021). [PubMed: 34181729]
127. Li J et al. Targeted mRNA demethylation using an engineered dCas13b–ALKBH5 fusion protein. Nucleic Acids Res. 48, 5684–5694 (2020). [PubMed: 32356894]
128. Wilson C, Chen PJ, Miao Z & Liu DR Programmable m^6A modification of cellular RNAs with a Cas13-directed methyltransferase. Nat. Biotechnol. 38, 1431–1440 (2020). [PubMed: 32601430]
129. Liu XM, Zhou J, Mao Y, Ji Q & Qian SB Programmable RNA N^6-methyladenosine editing by CRISPR–Cas9 conjugates. Nat. Chem. Biol. 15, 865–871 (2019). [PubMed: 31383972]
130. Rau K, Rosner L & Rentmeister A Sequence-specific m^6A demethylation in RNA by FTO fused to RCas9. RNA 25, 1311–1323 (2019). [PubMed: 31263003]
131. Chang C, Ma G, Cheung E & Hutchins AP A programmable system to methylate and demethylate N^6-methyladenosine (m^6A) on specific RNA transcripts in mammalian cells. J. Biol. Chem. 298, 102525 (2022). [PubMed: 36162509]
132. Rauch S, He C & Dickinson BC Targeted m^6A reader proteins to study epitranscriptomic regulation of single RNAs. J. Am. Chem. Soc. 140, 11974–11981 (2018). [PubMed: 30183280]
133. Mo J et al. TRADES: targeted RNA demethylation by SunTag system. Adv. Sci. 7, 2001402 (2020).
134. Zhao J, Li B, Ma J, Jin W & Ma X Photoactivatable RNA N^6-methyladenosine editing with CRISPR–Cas13. Small 16, e1907301 (2020). [PubMed: 32583968]
135. Xu M et al. CRISPR Cas13-based tools to track and manipulate endogenous telomeric repeat-containing RNAs in live cells. Front Mol. Biosci. 8, 785160 (2021). [PubMed: 35174207]
136. Chen M et al. Live imaging of RNA and RNA splicing in mammalian cells via the dCas13a–SunTag–BiFC system. Biosens. Bioelectron. 204, 114074 (2022). [PubMed: 35149451]
137. Yang LZ et al. Dynamic imaging of RNA in living cells by CRISPR–Cas13 systems. Mol. Cell 76, 981–997 (2019). [PubMed: 31757757]
138. Wang H et al. CRISPR-mediated live imaging of genome editing and transcription. Science 365, 1301–1305 (2019). [PubMed: 31488703]
139. Davis BJ & O'Connell MR Put on your para-spectacles: the development of optimized CRISPR–Cas13-based approaches to image RNA dynamics in real time. Mol. Cell 77, 207–209 (2020). [PubMed: 31951545]
140. Chen B et al. CRISPR-based RNA-binding protein mapping in live cells. Biochem. Biophys. Res. Commun. 583, 79–85 (2021). [PubMed: 34735883]
141. Zhang Z et al. Capturing RNA–protein interaction via CRUIS. Nucleic Acids Res. 48, e52 (2020). [PubMed: 32140725]
142. Han S et al. RNA–protein interaction mapping via MS2- or Cas13-based APEX targeting. Proc. Natl Acad. Sci. USA 117, 22068–22079 (2020). [PubMed: 32839320]
143. Montagud-Martínez R, Márquez-Costa R & Rodrigo G Programmable regulation of translation by harnessing the CRISPR–Cas13 system. Chem. Commun. 59, 2616–2619 (2023).
144. Charles EJ et al. Engineering improved Cas13 effectors for targeted post-transcriptional regulation of gene expression. Preprint at *bioRxiv* 10.1101/2021.05.26.445687 (2021).
145. Apostolopoulos A, Tsuiji H, Shichino Y & Iwasaki S CRISPRδ: dCas13-mediated translational repression for accurate gene silencing in mammalian cells. Preprint at *bioRxiv* 10.1101/2023.05.14.540671 (2023).
146. Otoupal PB, Cress BF, Doudna JA & Schoeniger JS CRISPR-RNAa: targeted activation of translation using dCas13 fusions to translation initiation factors. Nucleic Acids Res. 50, 8986–8998 (2022). [PubMed: 35950485]
147. Cao C et al. Enhancement of protein translation by CRISPR/dCasRx coupled with SINEB2 repeat of noncoding RNAs. Nucleic Acids Res. 51, e33 (2023). [PubMed: 36715335]
148. van Beljouw SPB et al. The gRAMP CRISPR–Cas effector is an RNA endonuclease complexed with a caspase-like peptidase. Science 373, 1349–1353 (2021). [PubMed: 34446442]
149. Yan WX et al. Functionally diverse type V CRISPR–Cas systems. Science 363, 88–91 (2019). [PubMed: 30523077]

150. Tng PYL et al. Cas13b-dependent and Cas13b-independent RNA knockdown of viral sequences in mosquito cells following guide RNA expression. Commun. Biol. 3, 413 (2020). [PubMed: 32737398]

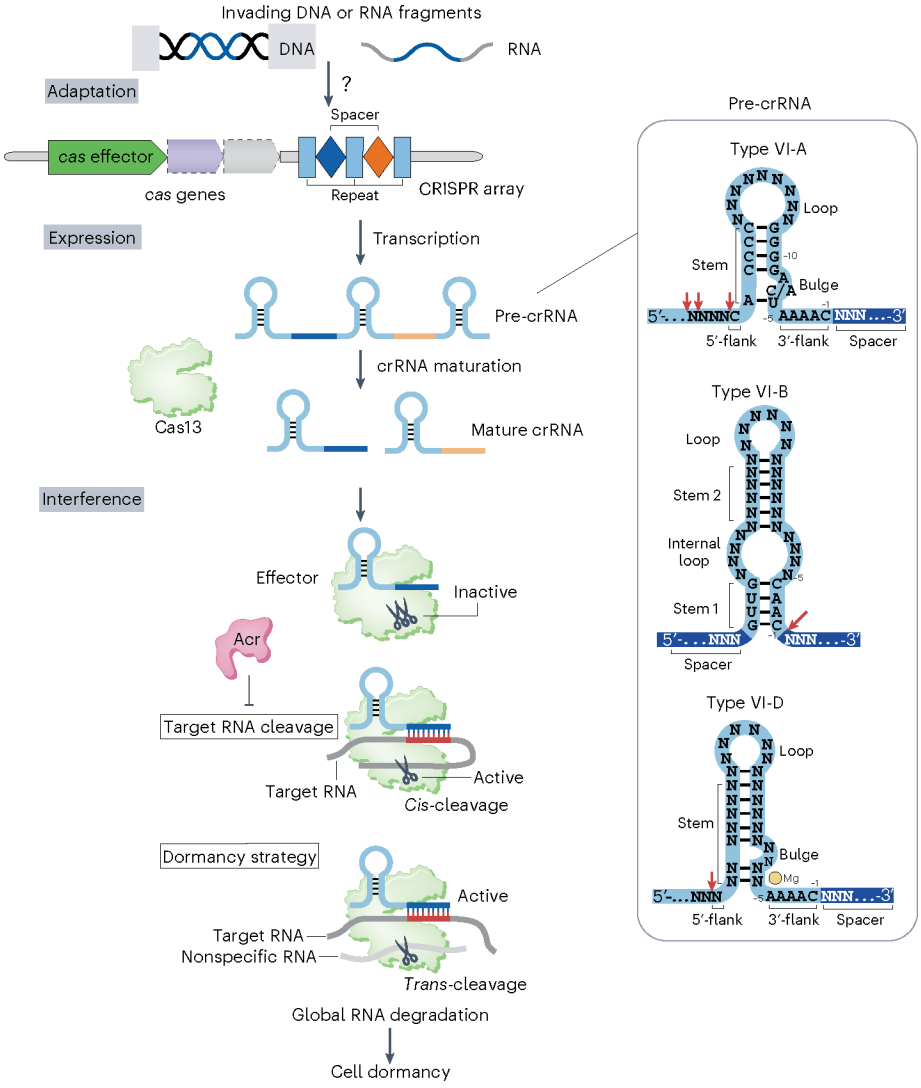

Fig. 1 |. Three stages of CRISPR–Cas13 adaptive immunity: adaptation, expression and interference.

CRISPR–Cas13 loci consist of a CRISPR array and neighboring *cas* genes. In the adaption stage, the adaptation machinery acquires fragments of invading mobile genetic elements and integrates them into the CRISPR array as new spacers, which generates heritable immunological memory. CRISPR repeats are represented as cyan rectangles, and spacers are represented as differently colored diamonds. The *cas1* and *cas2* genes, which encode adaptation modules, are missing in most Cas13 loci. How these Cas13 systems acquire new spacers remains unclear. During the CRISPR expression stage, the CRISPR array is transcribed as pre-crRNA and is processed into mature crRNA by Cas13, such that each crRNA carries a single spacer flanked with a part of the direct repeat on one side. The topologies of pre-crRNA in types VI-A, VI-B and VI-D systems, highlighting the conserved sequences and secondary structures, as well as the differences among different subtypes are shown in the zoomed-in box. Pre-crRNA processing sites are indicated by red arrows. The mature crRNA assembles with its effector protein Cas13 to form a surveillance complex that recognizes and degrades foreign genetic elements complementary to the crRNA spacer

during interference. At the interference stage, guide–target base-pairing requirements enable sequence-specific targeting and lead to activation of Cas13 for the cleavage of target RNA at promiscuous positions outside the pairing region. Additionally, upon target RNA recognition, Cas13 causes collateral RNase activity against environmental substrate RNA, which induces cell dormancy. Acrs encoded by bacteriophages can directly inactivate Cas13 and prevent target cleavage.

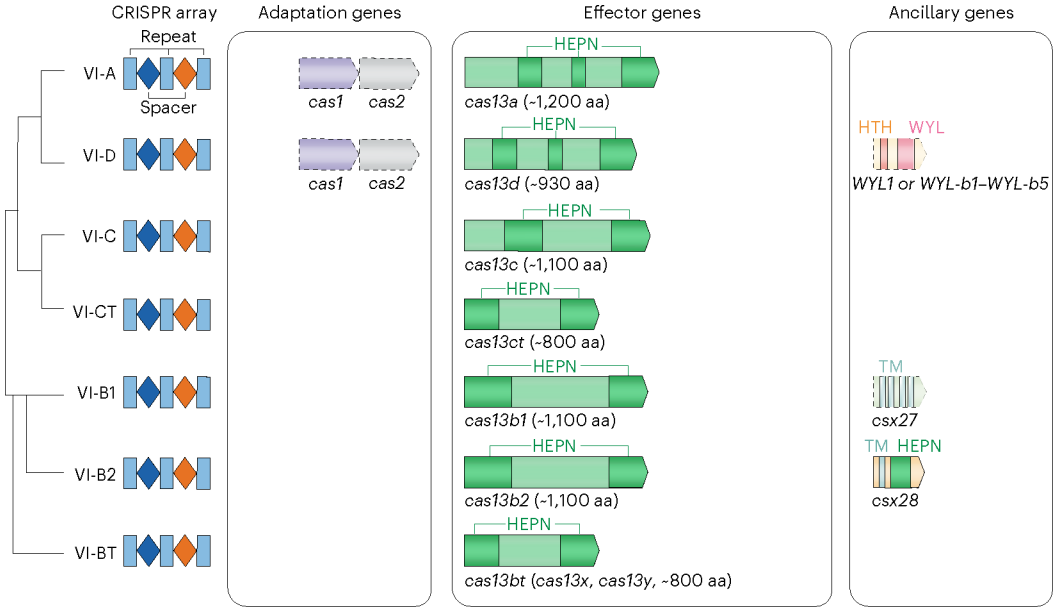

Fig. 2 |. Functional module organization of CRISPR type VI Cas13 loci.

The functional modules involved in adaptation, expression and interference for each subtype are illustrated in the inserted panels. The approximate positions of the two HEPN domains are indicated in dark green within each effector Cas13a (C2c2), Cas13b (C2c6), Cas13c (C2c7), Cas13d (CasRx), Cas13bt (further classified as Cas13X and Cas13Y) and Cas13ct proteins. The average sizes of Cas13 proteins are indicated under the corresponding genes, among which Cas13d (~930 amino acids (aa)) and Cas13bt and Cas13ct (~800 amino acids) proteins are relatively smaller than their Cas13a–Cas13c protein counterparts (larger than 1,100 amino acids). Genes encoding Cas1, Cas2, Csx27, Csx28 and WYL domain proteins are found only in some species in a set of indicated subtypes and are marked by dashed outlines. The dendrogram on the left of the Cas13 systems is adapted from refs. 34,38,45 and shows the potential evolutionary relationships. The branch lengths are not scaled and do not indicate evolutionary distances. HTH, helix–turn–helix. TM, transmembrane.

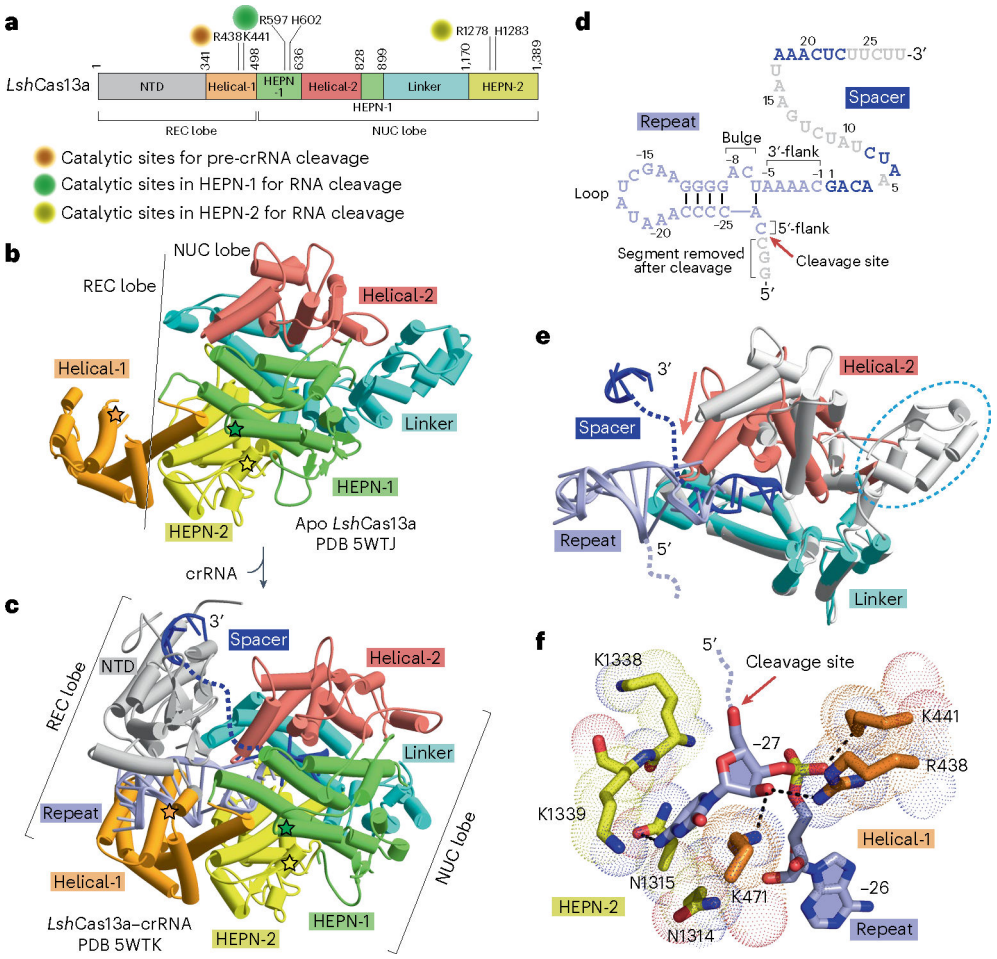

Fig. 3 |. Mechanisms of crRNA recognition and maturation in type VI-A systems.

a, Schematic representation of the domain architecture of *Lsh*Cas13a. The catalytic sites for pre-crRNA cleavage and target RNA cleavage are labeled. **b**,**c**, Overall structures of *Lsh*Cas13a in apo (**b**; PDB 5WTJ) and crRNA-bound (**c**; PDB 5WTK) states. The line indicates the boundary between the REC lobe and the NUC lobe. The NTD domain in the REC lobe, which cannot be traced in the apo form, is clearly visible in the crRNA-bound form. The bound crRNA is embedded in the Cas13 scaffold with the entire repeat segment traceable, but only some segments of the spacer are detectable in the structure of the complex. The direct repeat and the spacer are colored in light blue and dark blue, while disordered regions are indicated as dashed lines. The catalytic residues for pre-crRNA cleavage are indicated by orange stars, while the R-$X_{4–6}$-H motifs in the two HEPN domains for target RNA cleavage are indicated by green and yellow stars, respectively. **d**, Topology showing crRNA in the Cas13a-bound state on binary complex formation. Loop, flank and bulge elements are labeled. Nucleotides not observed in the structure are colored in gray. The pre-crRNA processing site is indicated by a red arrow. **e**, Domain movements induced by crRNA loading. The structure of Cas13a in the apo state (in silver) is superimposed with the structure of Cas13a in the crRNA-bound state (in color). The major domain movements occur in the helical-2 domain that shifts toward the linker domain. A portion of the linker

domain is disordered in the crRNA-bound state, which is indicated as a cyan dashed circle. **f**, Detailed interaction between the pre-crRNA cleavage site nucleotide C(−27) and Cas13a.

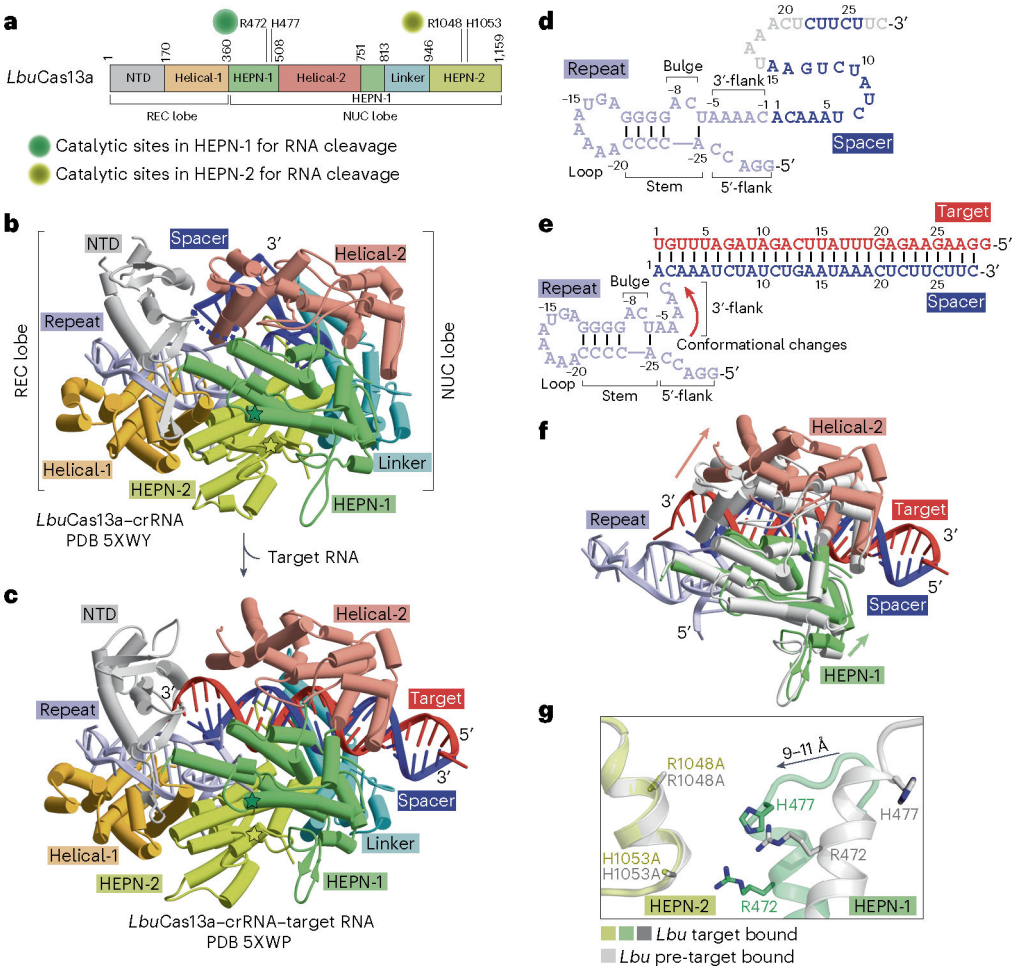

Fig. 4 |. Mechanisms of target RNA recognition in type VI-A systems.

a, Schematic representation of the domain architecture of *Lbu*Cas13a. The catalytic sites in the pair of HEPN domains for target RNA cleavage are indicated. **b**,**c**, Overall structures of the *Lbu*Cas13a–crRNA binary complex in the absence (**b**, pre-target bound; PDB 5XWY) and presence (**c**, target bound; PDB 5XWP) of target RNA. The REC and NUC lobes are labeled. The R-$X_{4–6}$-H motifs in the two HEPN domains for target cleavage are indicated by colored stars. **d**,**e**, Topology of crRNA (**d**) and crRNA–target RNA (**e**) in the *Lbu*Cas13a binary and ternary complexes. The direct repeat, spacer and target RNA are colored in light blue, dark blue and red, respectively. The loop, flank and bulge elements of crRNA are labeled. Nucleotides not observed in the structure are colored in gray. The conformational change in the 3′-flank of the crRNA direct repeat is indicated by a red arrow. The 3′-flank region (−3 to −1) of the direct repeat of *Lbu*Cas13a–crRNA moves toward the stem loop as indicated by red arrows. **f**, Domain movements in the Cas13a–crRNA binary complex induced by bound target RNA on ternary complex formation. The structure of *Lbu*Cas13a in the pre-target RNA-bound state (in silver) is superimposed with that in the target RNA-bound state (in color). The major domain movements occur in the helical-2 and HEPN-1 domains and are indicated by colored arrows. **g**, Conformational changes in catalytic residues of the pair of HEPN domains on proceeding from the Cas13a–crRNA

binary complex (in silver) to the ternary complex with added target RNA (in color). Target RNA loading induces the formation of a composite catalytic pocket involving a pair of HEPN domains (in color). *Lbu*, *Lbu*Cas13a.

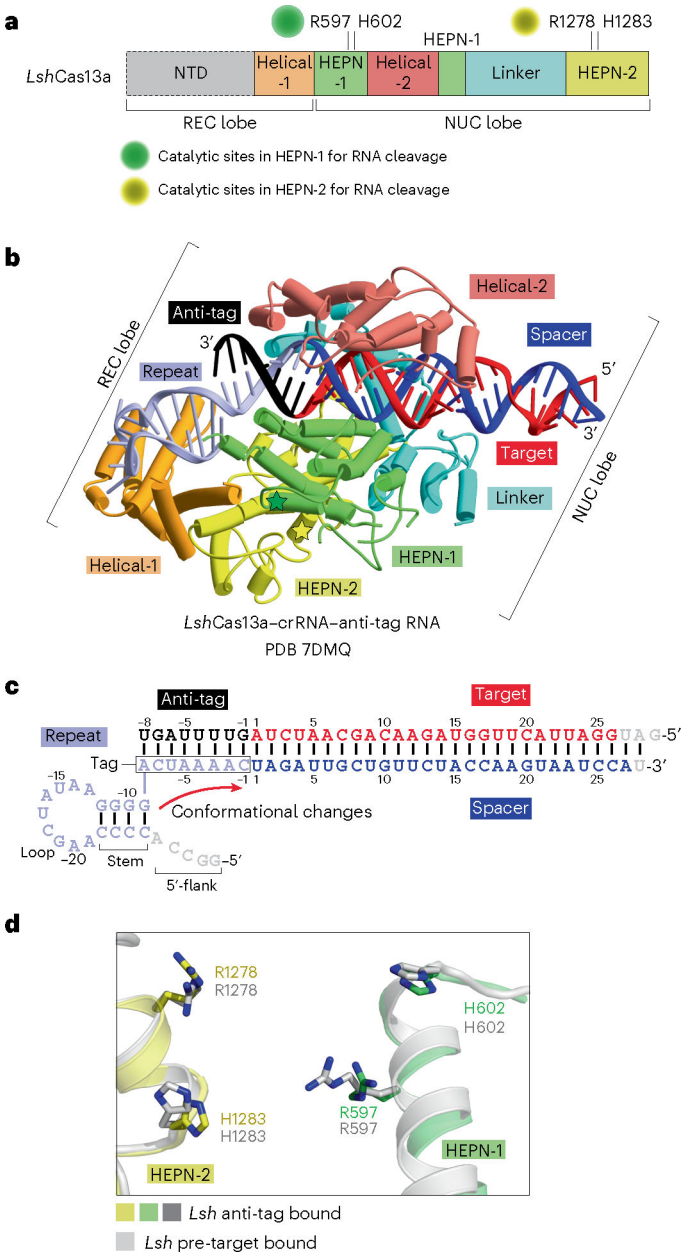

Fig. 5 |. Mechanism of self–non-self-discrimination in type VI-A systems.

a, Schematic representation of *Lsh*Cas13a domain architecture. **b**, Overall structure of the *Lsh*Cas13a–crRNA binary complex bound to target RNA (PDB 7DMQ) in which the target RNA anti-tag segment pairs with the crRNA tag segment. The NTD domain is disordered as indicated as the dashed box in **a**. **c**, Topology showing pairing alignment between crRNA and anti-tag containing target RNA. The 8-nucleotide tag segment is highlighted with a black box. The 8-nucleotide anti-tag and 28-nucleotide target regions of target RNA are colored in black and red, respectively. The conformational changes of the tag segment are indicated by a red arrow. **d**, Comparison of catalytic residues of the pair of HEPN domains on proceeding from the Cas13a–crRNA binary complex (in silver) to the ternary complex (in

color) with added anti-tag target RNA. The catalytic residues remain apart from each other, indicating that Cas13a is inactive after binding with anti-tag target RNA. Lsh, *Lsh*Cas13a.

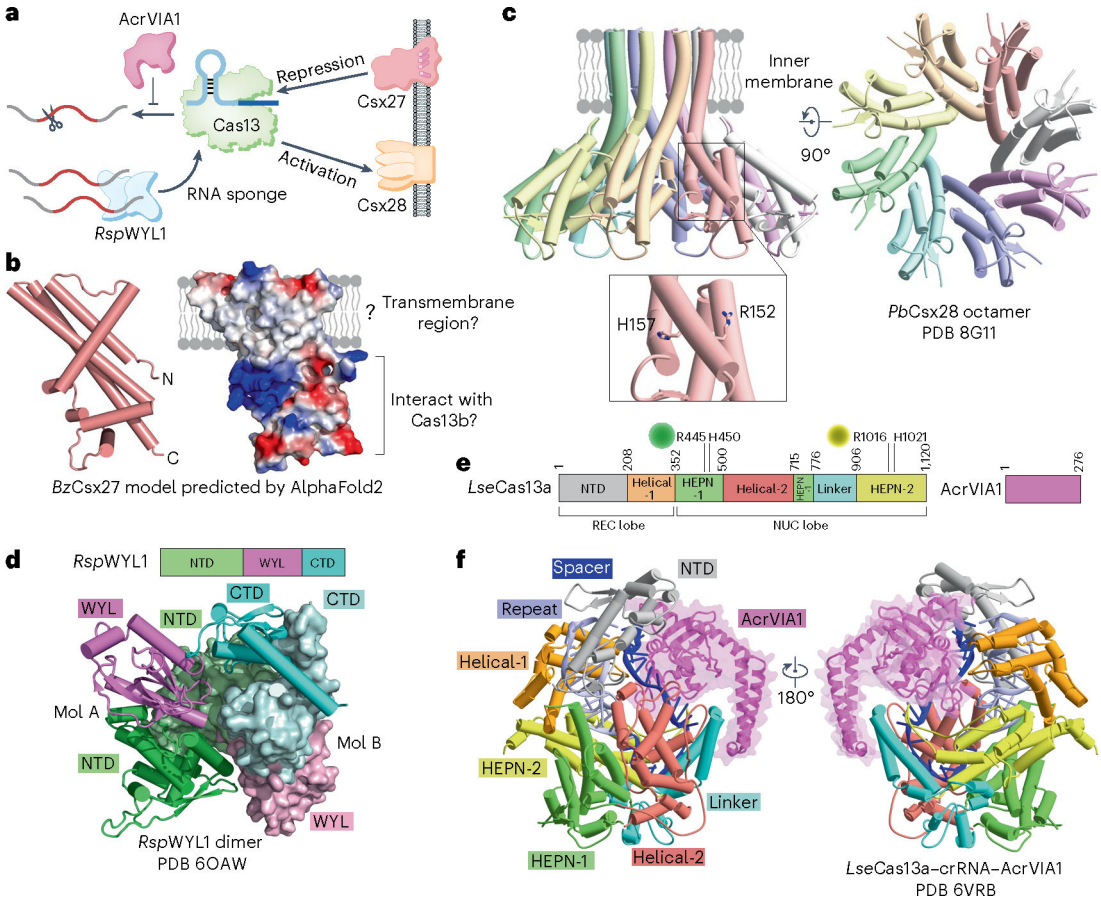

Fig. 6 |. Modulation mechanisms of type VI systems involving anti-CRISPRs and accessory proteins.

a, Proposed modulation mechanisms mediated by anti-CRISPRs and accessory proteins. **b**, AlphaFold2-predicted overall structure (left) and electrostatic surface (right) of *Bz*Csx27. The hydrophobic surface might be associated with membrane. **c**, Overall structure of the *Pb*Csx28 octamer (PDB 8GI1). Transmembrane regions are indicated. The predicted key residues R152 and H157 in the R-$X_{4–6}$-H motif are shown as a stick model in the zoomed-in box. **d**, Overall domain alignment and structure of the *Rsp*WYL1 dimer (top; PDB 6OAW). Monomer A (Mol A) is shown in a ribbon mode, and monomer B (Mol B) is shown as a surface mode. **e**, Schematic representation of the domains of *Lse*Cas13a and AcrVIA1. **f**, Two views of a ribbon diagram showing Acr protein AcrVIA1 (in surface) bound to *Lse*Cas13–crRNA (in ribbon) (PDB 6VRB). AcrVIA1 directly binds to and interacts with distinct domains of Cas13, thereby blocking access to target RNA.

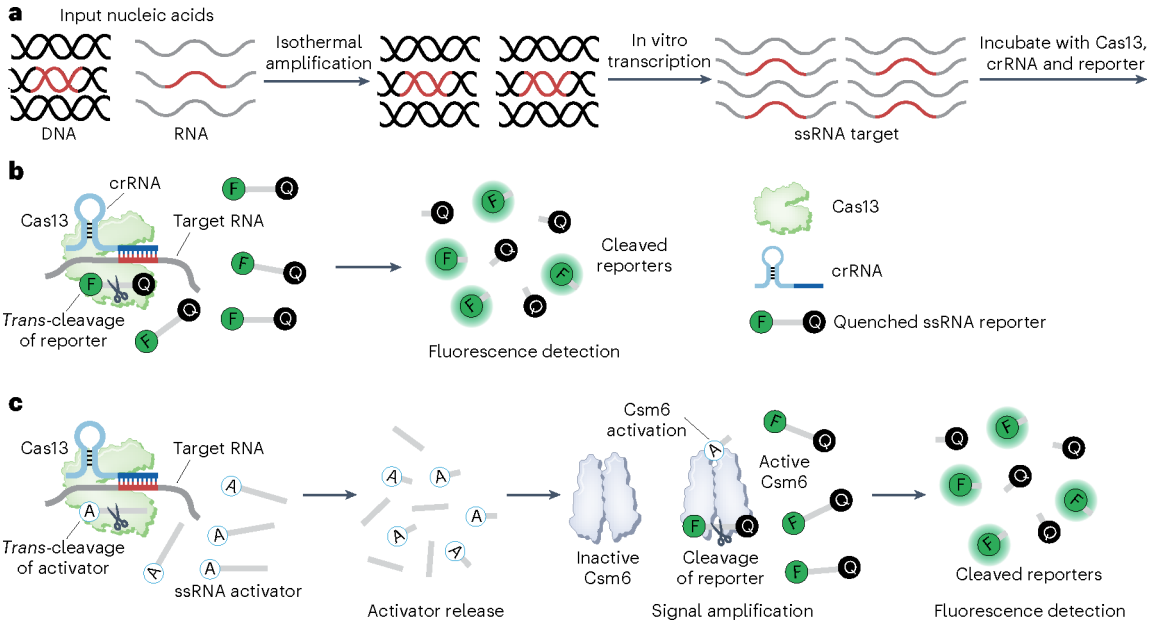

Fig. 7 |. Active Cas13-based RNA-targeting technologies.

a, DNA or RNA samples are amplified by isothermal amplification and then transcribed into ssRNA. **b**, Binding of the crRNA to the complementary target sequence activates Cas13 collateral cleavage of quenched fluorescent ssRNA reporters, thereby releasing fluorescence signal. **c**, Schematic of Cas13–Csm6-based nucleic acid detection.

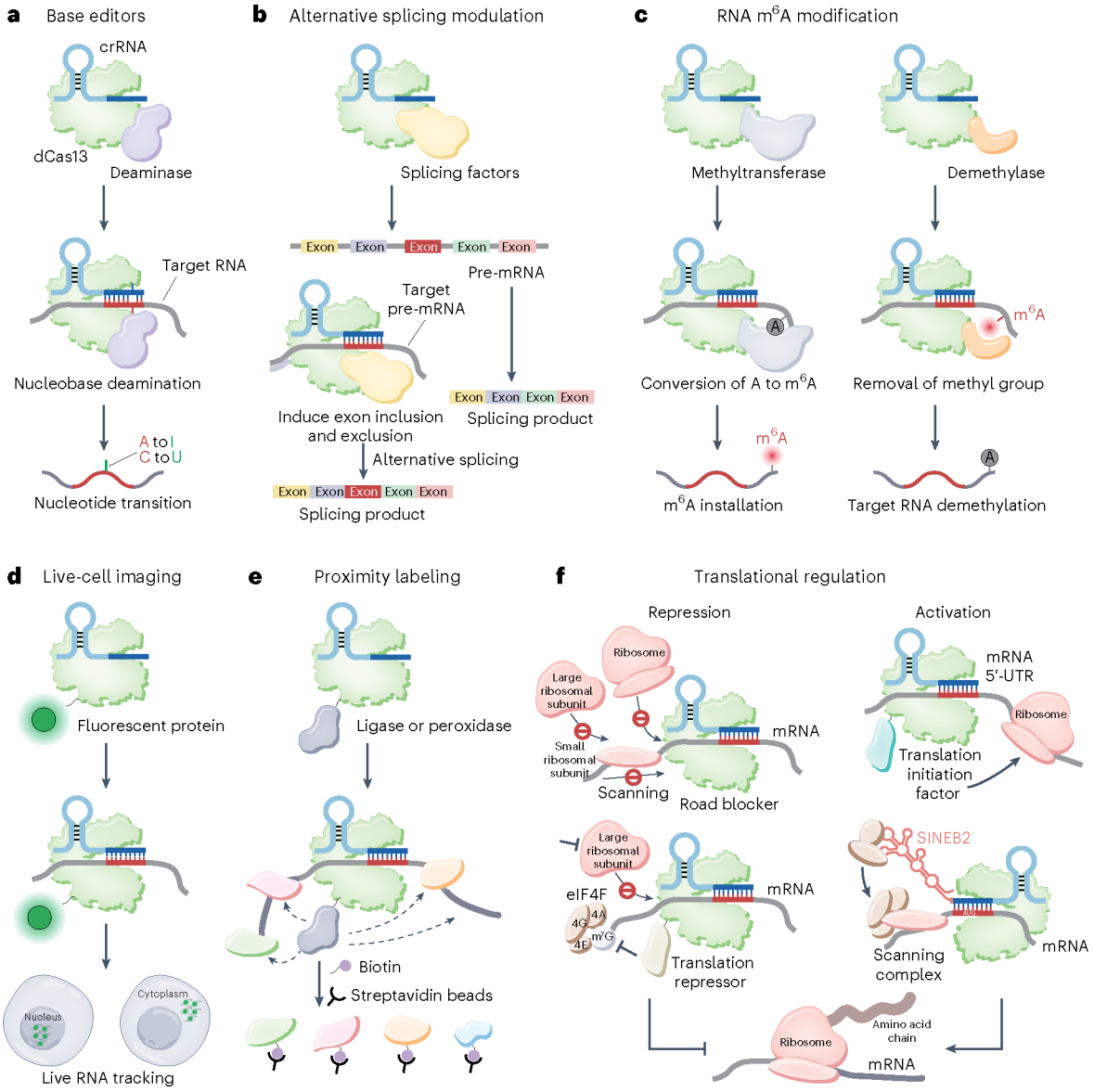

Fig. 8 |. dCas13-based RNA manipulation technologies.

a, RNA base editing. The dCas13–deaminase fusion can be used for site-specific nucleotide conversion. **b**, Programmable alternative splicing modulation. dCas13 fused to splicing factors can be used for pre-mRNA alternative splicing modulation to generate a customized splicing product. **c**, Programmable RNA m^{6}A modification regulation. dCas13 fused to methyltransferase complex (left) or demethylase (right) can mediate the m^{6}A methylation levels of target RNA. **d**, Endogenous RNA imaging and tracking. dCas13 fused to a fluorescent protein enables the visualization of RNA in live cells. By fusing different localization signals with Cas13, target RNA can be transported to the desired cellular location, such as the nucleus and the cytoplasm. **e**, Cas13-based proximity labeling. dCas13 fused with ligase or peroxidase can be applied to label proximal proteins with biotin and facilitate the discovery of new proteins interacting with target RNA. **f**, dCas13 recruited to mRNA may physically abrogate ribosome binding and movement, thereby impeding

translation initiation and elongation. dCas13 fused with a translational repressor provides an alternative suppression mechanism upon m^7G cap binding, increasing translational repression efficiency. dCas13 fused with a translational initiation factor targeting the 5′-UTR of mRNA enables the recruitment of ribosomal subunits and thus presumably increases translation initiation. Through ribosome recruitment by the SINEB2 element, the dCasRx–SINEB2 system allows for translation activation by targeting the initiation region around the AUG start codon. eIF4, eukaryotic initiation factor 4.